undetectable in these normal and leukemic B-cell lines. Moreover, the *LMO2* gene expression level was markedly down-regulated during the transition from CD19-negative to CD19-positive population in the cord blood $CD34^+$MNCs. These data are in agreement with the down-regulation of *LMO2* gene expression during the early phase in the normal progression of B-cell development.[19] Of note, gene silencing of *LMO2* by the introduction of shRNA using lentivirus vector induced specific cell death. Interestingly, a recent analysis by Natkunam et al[15] demonstrated that the majority of CD10-positive germinal center B cells coexpressed LMO2 while $CD79a^+$ plasma cells lacked LMO2 expression, suggesting the association of LMO2 down-regulation with normal B-cell development. These observations seem to be in agreement with the assumption that aberrant expression of LMO2 is involved in the maturation arrest of t(17;19)-ALL cells at the immature B-precursor stage. Taken together, LMO2 expression is down-regulated during the normal development of both T cells and B cells, and its aberrant expression promotes cell survival of immature lymphocytes, which subsequently contributes to leukemogenesis of both T-ALL and B-precursor ALL. In this context, it should be noted that approximately one-fourth of non-t(17;19) B-precursor ALL cell lines expressed LMO2 at an equivalent level to that in t(17;19)-ALL cell lines, suggesting that LMO2 might also play a role, at least in part, in the leukemogenesis of other types of B-precursor ALL. Finally, considering the dismal outcome of conventional chemotherapy for t(17;19)-ALL cases,[45] the development of new therapeutic modalities is urgently needed. Here we demonstrated that gene silencing of *LMO2* using shRNA specifically induced cell death of t(17;19)-ALL cells. Thus, there is a possibility that aberrantly expressed LMO2 in t(17;19)-ALL might become a possible target for therapy.

Authorship

Contribution: K.H. performed most of experiments and analyzed the data; T. Inukai designed the project, analyzed the data, and wrote the manuscript; J.K. and Y.F. performed shRNA analysis; T. Ikawa, H. Kawamoto, H. Kurosawa, A.T.L., and H.M. provided tools for analysis; S.H.O., B.G, N.K., Y.M., and H.O. performed gene expression analysis; K.A., X.Z., I.K., H.H., K.K., and K.G. performed analysis of cell line; T. Inaba wrote the manuscript; and K.S. supervised the project and wrote the manuscript.

Conflict-of-interest disclosure: The authors declare no competing financial interests.

Correspondence: Dr Takeshi Inukai, Department of Pediatrics, School of Medicine, University of Yamanashi, 1110 Shimokato, Chuo, Yamanashi 409-3898, Japan; e-mail: tinukai@yamanashi.ac.jp.

References

1. Rabbitts TH. Chromosomal translocations in human cancer. *Nature.* 1994;372(6502):143-149.
2. Look AT. Oncogenic transcription factors in the human acute leukemias. *Science.* 1997; 278(5340):1059-1064.
3. Boehm T, Foroni L, Kaneko Y, Perutz MF, Rabbitts TH. The rhombotin family of cysteine-rich LIM-domain oncogenes: distinct members are involved in T-cell translocations to human chromosomes 11p15 and 11p13. *Proc Natl Acad Sci U S A.* 1991;88(10):4367-4371.
4. Royer-Pokora B, Loos U, Ludwig WD. TTG-2, a new gene encoding a cysteine-rich protein with the LIM motif, is overexpressed in acute T-cell leukaemia with the t(11;14)(p13;q11). *Oncogene.* 1991;6(10):1887-1893.
5. Wadman I, Li J, Bash RO, et al. Specific in vivo association between the bHLH and LIM proteins implicated in human T cell leukemia. *EMBO J.* 1994;13(20):4831-4839.
6. Wadman IA, Osada H, Grutz GG, et al. The LIM-only protein Lmo2 is a bridging molecule assembling an erythroid, DNA-binding complex which includes the TAL1, E47, GATA-1 and Ldb1/NLI proteins. *EMBO J.* 1997;16(11):3145-3157.
7. Agulnick AD, Taira M, Breen JJ, Tanaka T, Dawid IB, Westphal H. Interactions of the LIM-domain-binding factor Ldb1 with LIM homeodomain proteins. *Nature.* 1996;384(6606):270-272.
8. Grütz GG, Bucher K, Lavenir I, Larson T, Larson R, Rabbitts TH. The oncogenic T cell LIM-protein Lmo2 forms part of a DNA-binding complex specifically in immature T cells. *EMBO J.* 1998; 17(16):4594-4605.
9. Warren AJ, Colledge WH, Carlton MB, Evans MJ, Smith AJ, Rabbitts TH. The oncogenic cysteine-rich LIM domain protein rbtn2 is essential for erythroid development. *Cell.* 1994;78(1):45-57.
10. Yamada Y, Warren AJ, Dobson C, Forster A, Pannell R, Rabbitts TH. The T cell leukemia LIM protein Lmo2 is necessary for adult mouse hematopoiesis. *Proc Natl Acad Sci U S A.* 1998;95(7): 3890-3895.
11. Yamada Y, Pannell R, Forster A, Rabbitts TH. The oncogenic LIM-only transcription factor Lmo2 regulates angiogenesis but not vasculogenesis in mice. *Proc Natl Acad Sci U S A.* 2000;97(1):320-324.
12. Akashi K, He X, Chen J, Iwasaki H, Niu C, Steenhard B, Zhang J, Haug J, Li L. Transcriptional accessibility for genes of multiple tissues and hematopoietic lineages is hierarchically controlled during early hematopoiesis. *Blood.* 2003; 101(2):383-389.
13. Alizadeh AA, Eisen MB, Davis RE, et al. Distinct types of diffuse large B-cell lymphoma identified by gene expression profiling. *Nature.* 2000; 403(6769):503-511.
14. Lossos IS, Czerwinski DK, Alizadeh AA, et al. Prediction of survival in diffuse large-B-cell lymphoma based on the expression of six genes. *N Engl J Med.* 2004;350(18):1828-1837.
15. Natkunam Y, Zhao S, Mason DY, et al. The oncoprotein LMO2 is expressed in normal germinal-center B cells and in human B-cell lymphomas. *Blood.* 2007;109(4):1636-1642.
16. McCormack MP, Forster A, Drynan L, Pannell R, Rabbitts TH. The LMO2 T-cell oncogene is activated via chromosomal translocations or retroviral insertion during gene therapy but has no mandatory role in normal T-cell development. *Mol Cell Biol.* 2003;23(24):9003-9013.
17. Fisch P, Boehm T, Lavenir I, et al. T-cell acute lymphoblastic lymphoma induced in transgenic mice by the RBTN1 and RBTN2 LIM-domain genes. *Oncogene.* 1992;7(12):2389-2397.
18. Larson RC, Fisch P, Larson TA, et al. T cell tumours of disparate phenotype in mice transgenic for Rbtn-2. *Oncogene.* 1994;9(12):3675-3681.
19. Larson RC, Osada H, Larson TA, Lavenir I, Rabbitts TH. The oncogenic LIM protein Rbtn2 causes thymic developmental aberrations that precede malignancy in transgenic mice. *Oncogene.* 1995;11(5):853-862.
20. Neale GA, Rehg JE, Goorha RM. Ectopic expression of rhombotin-2 causes selective expansion of CD4-CD8- lymphocytes in the thymus and T-cell tumors in transgenic mice. *Blood.* 1995;86(8): 3060-3071.
21. Hacein-Bey-Abina S, Von Kalle C, Schmidt M, et al. LMO2-associated clonal T cell proliferation in two patients after gene therapy for SCID-X1. *Science.* 2003;302(5644):415-419.
22. McCormack MP, Rabbitts TH. Activation of the T-cell oncogene LMO2 after gene therapy for X-linked severe combined immunodeficiency. *N Engl J Med.* 2004;350(9):913-922.
23. Royer-Pokora B, Rogers M, Zhu TH, Schneider S, Loos U, Bolitz U. The TTG-2/RBTN2 T cell oncogene encodes two alternative transcripts from two promoters: the distal promoter is removed by most 11p13 translocations in acute T cell leukaemia's (T-ALL). *Oncogene.* 1995;10(7):1353-1360.
24. Landry JR, Kinston S, Knezevic K, Donaldson IJ, Green AR, Gottgens B. Fli1, Elf1, and Ets1 regulate the proximal promoter of the LMO2 gene in endothelial cells. *Blood.* 2005;106(8):2680-2687.
25. Crable SC, Anderson KP. A PAR domain transcription factor is involved in the expression from a hematopoietic-specific promoter for the human LMO2 gene. *Blood.* 2003;101(12):4757-4764.
26. Inaba T, Roberts WM, Shapiro LH, et al. Fusion of the leucine zipper gene HLF to the E2A gene in human acute B-lineage leukemia. *Science.* 1992; 257(5069):531-534.
27. Hunger SP, Ohyashiki K, Toyama K, Cleary ML. Hlf, a novel hepatic bZIP protein, shows altered DNA-binding properties following fusion to E2A in t(17;19) acute lymphoblastic leukemia. *Genes Dev.* 1992;6(9):1608-1620.
28. Mueller CR, Maire P, Schibler U. DBP, a liver-enriched transcriptional activator, is expressed late in ontogeny and its tissue specificity is determined posttranscriptionally. *Cell.* 1990;61(2):279-291.
29. Drolet D, Scully K, Simmons D, et al. TEF, a transcription factor expressed specifically in the anterior pituitary during embryogenesis, defines a new class of leucine zipper proteins. *Genes Dev.* 1991;5(10):1739-1753.
30. Yoshihara T, Inaba T, Shapiro LH, Kato JY, Look AT. E2A-HLF-mediated cell transformation requires both the trans-activation domains of E2A and the leucine zipper dimerization domain of HLF. *Mol Cell Biol.* 1995;15(6):3247-3255.

31. Inukai T, Inaba T, Yoshihara T, Look AT. Cell transformation mediated by homodimeric E2A-HLF transcription factors. *Mol Cell Biol.* 1997;17(3):1417-1424.
32. Inaba T, Inukai T, Yoshihara T, et al. Reversal of apoptosis by the leukaemia-associated E2A-HLF chimaeric transcription factor. *Nature.* 1996;382(6591):541-544.
33. Inukai T, Inaba T, Ikushima S, Look AT. The AD1 and AD2 transactivation domains of E2A are essential for the antiapoptotic activity of the chimeric oncoprotein E2A-HLF. *Mol Cell Biol.* 1998;18(10):6035-6043.
34. Inukai T, Inaba T, Dang J, et al. TEF, an antiapoptotic bZIP transcription factor related to the oncogenic E2A-HLF chimera, inhibits cell growth by down-regulating expression of the common beta chain of cytokine receptors. *Blood.* 2005;105(11):4437-4444.
35. Smith KS, Rhee JW, Naumovski L, Cleary ML. Disrupted differentiation and oncogenic transformation of lymphoid progenitors in E2A-HLF transgenic mice. *Mol Cell Biol.* 1999;19(6):4443-4451.
36. Honda H, Inaba T, Suzuki T, et al. Expression of E2A-HLF chimeric protein induced T-cell apoptosis, B-cell maturation arrest, and development of acute lymphoblastic leukemia. *Blood.* 1999;93(9):2780-2790.
37. Inaba T, Shapiro LH, Funabiki T, et al. DNA-binding specificity and trans-activating potential of the leukemia-associated E2A-hepatic leukemia factor fusion protein. *Mol Cell Biol.* 1994;14(5):3403-3413.
38. Hunger SP, Brown R, Cleary ML. DNA-binding and transcriptional regulatory properties of hepatic leukemia factor (HLF) and the t(17;19) acute lymphoblastic leukemia chimera E2A-HLF. *Mol Cell Biol.* 1994;14(9):5986-5996.
39. Inukai T, Zhang X, Goto M, et al. Resistance of infant leukemia with MLL rearrangement to tumor necrosis factor-related apoptosis-inducing ligand: a possible mechanism for poor sensitivity to antitumor immunity. *Leukemia.* 2006;20(12):2119-2129.
40. Uno K, Inukai T, Kayagaki N, et al. TNF-related apoptosis-inducing ligand (TRAIL) frequently induces apoptosis in Philadelphia chromosome-positive leukemia cells. *Blood.* 2003;101(9):3658-3667.
41. Rubinson DA, Dillon CP, Kwiatkowski AV, et al. A lentivirus-based system to functionally silence genes in primary mammalian cells, stem cells and transgenic mice by RNA interference. *Nat Genet.* 2003;33(3):401-406.
42. Kikuchi J, Shimizu R, Wada T, et al. E2F-6 suppresses growth-associated apoptosis of human hematopoietic progenitor cells by counteracting proapoptotic activity of E2F-1. *Stem Cells.* 2007;25(10):2439-2447.
43. Garcia IS, Kaneko Y, Gonzalez-Sarmiento R, et al. A study of chromosome 11p13 translocations involving TCR beta and TCR delta in human T cell leukaemia. *Oncogene.* 1991;6(4):577-582.
44. Van Vlierberghe P, van Grotel M, Beverloo HB, et al. The cryptic chromosomal deletion del(11)(p12p13) as a new activation mechanism of LMO2 in pediatric T-cell acute lymphoblastic leukemia. *Blood.* 2006;108(10):3520-3529.
45. Inukai T, Hirose K, Inaba T, Kurosawa H, et al. Hypercalcemia in childhood acute lymphoblastic leukemia: frequent implication of parathyroid hormone-related peptide and E2A-HLF from translocation 17;19. *Leukemia.* 2007;21(2):288-296.

THE JOURNAL OF BIOLOGICAL CHEMISTRY VOL. 286, NO. 7, pp. 5589–5598, February 18, 2011

The Dynactin Complex Maintains the Integrity of Metaphasic Centrosomes to Ensure Transition to Anaphase*[S]

Received for publication, July 22, 2010, and in revised form, December 14, 2010 Published, JBC Papers in Press, December 16, 2010, DOI 10.1074/jbc.M110.167742

Yuko Ozaki, Hirotaka Matsui, Akiko Nagamachi, Hiroya Asou, Daisuke Aki, and Toshiya Inaba[1]

From the Department of Molecular Oncology and Leukemia Program Project, Research Institute for Radiation Biology and Medicine, Hiroshima University, Hiroshima 734-8553, Japan

The dynactin complex is required for activation of the dynein motor complex, which plays a critical role in various cell functions including mitosis. During metaphase, the dynein-dynactin complex removes spindle checkpoint proteins from kinetochores to facilitate the transition to anaphase. Three components (p150^{Glued}, dynamitin, and p24) compose a key portion of the dynactin complex, termed the projecting arm. To investigate the roles of the dynactin complex in mitosis, we used RNA interference to down-regulate p24 and p150^{Glued} in human cells. In response to p24 down-regulation, we observed cells with delayed metaphase in which chromosomes frequently align abnormally to resemble a "figure eight," resulting in cell death. We attribute the figure eight chromosome alignment to impaired metaphasic centrosomes that lack spindle tension. Like p24, RNA interference of p150^{Glued} also induces prometaphase and metaphase delays; however, most of these cells eventually enter anaphase and complete mitosis. Our findings suggest that although both p24 and p150^{Glued} components of the dynactin complex contribute to mitotic progression, p24 also appears to play a role in metaphase centrosome integrity, helping to ensure the transition to anaphase.

The dynein-dynactin complex, a minus end-directed microtubule-based motor, carries out diverse transport activities indispensable for various cell functions and behaviors (Ref. 1 and references therein). For instance, the dynein-dynactin complex transports giant centrosomal scaffold proteins such as CG-NAP/AKAP450 and NuMA and induces smooth progression through mitosis. This motor complex also contributes to the transition from metaphase to anaphase: To ensure that each daughter cell receives only one chromosome set, the spindle assembly checkpoint blocks entry into anaphase until kinetochores on sister chromatids are attached to opposite spindle poles. Once this condition is achieved, the dynein-dynactin motor induces passage through the spindle checkpoint by removing critical checkpoint proteins (such as BubR1 or Mad2) from kinetochores.

* This work was supported by grants-in-aid for scientific research from the Ministry of Education, Culture, Sports, Science and Technology of Japan.
[S] The on-line version of this article (available at http://www.jbc.org) contains supplemental Movies 1–3.
[1] To whom correspondence should be addressed: 1-2-3 Kasumi, Minami-ku, Hiroshima 734-8553, Japan. Fax: 81-82-256-7103; E-mail: tinaba@hiroshima-u.ac.jp.

Dynactin is composed of 10 subunit proteins that are required for dynein activation (2) and references therein). Three proteins among them, p150^{Glued} (dynactin 1), dynamitin (p50 and dynactin 2), and p24 (dynactin 3) (3, 4), constitute a flexible and extendable structure (the projecting arm) that associates directly with microtubules and the dynein complex.

Each dynactin molecule contains two copies of p150^{Glued} and p24 and four copies of dynamitin. All three proteins are evolutionarily conserved from yeast to mammalian cells (5, 6), suggesting that these components are essential for the formation of a functional projecting arm. Within this substructure, p150^{Glued} is sufficient for binding to dynein and for traversing the microtubule lattice, whereas dynamitin also plays a critical role in association with the dynein complex and in promotion of dynein-based movement. It is noteworthy that overexpression of dynamitin disrupts dynactin structure (7). Although the mechanism underlying this disruption is yet to be elucidated, dynamitin overexpression has been the major tool in molecular biology for down-regulation of dynactin function (2). Indeed, dynamitin overexpression was used to verify involvement of the dynactin complex in the spindle checkpoint silencing that induces metaphase arrest/delay (8).

In contrast to p150^{Glued} or dynamitin, little is known about the role of the p24 subunit in mitosis. Although Ldb18 (a *Saccharomyces cerevisiae* homolog of p24) is essential for attachment of p150^{Glued} to dynamitin and to the remainder of the dynactin complex (6), low amino acid identity between Ldb18 and human p24 (16.9%) does not favor speculation on the roles of mammalian p24.

RNAi is currently the most useful method for down-regulating the expression of a specific gene. Although several authors report successful suppression of p150^{Glued} using siRNA or shRNA (8–10), their papers did not describe any mitotic abnormalities in cells expressing reduced levels of p150^{Glued}. Moreover, there have been no reports of p24 down-regulation using the RNAi method. In this report, we use RNAi to down-regulate p24 and p150^{Glued} proteins in human cells. Our results demonstrate that cells expressing reduced levels of either p24 or p150^{Glued} both show severe metaphase delay but that other mitotic disturbances differ between the two suppressed genes.

EXPERIMENTAL PROCEDURES

Cell Culture and Transfection of siRNA—HeLa, U2OS, and HEK 293 cell lines and their derivative cells were cultured in Dulbecco's modified Eagle's medium supplemented with 10% FBS. siRNA oligonucleotides for p150^{Glued} (siRNA-p150, 5′-

GACTTCACCCCTTGATTAA-3′; siRNA-p150b, 5′-CCACCACCAAAGGUUAAGU-3′) (10) or p24 (siRNA-p24, 5′-CCGCATTGCCATACCTGAT-3; siRNA-p24b, 5′-GCUACUUUGCCAGCUAGAG-3′) were transfected at a concentration of 100 nM into HeLa(tc), a HeLa subline (11) or U2OS cells using Oligofectamine (Invitrogen), otherwise indicated in text and figure legends. Dead cells were identified using the trypan blue dye exclusion test. p24 and H2B-GFP were expressed using the pcDNA3 expression vector (Invitrogen).

Rescue Experiments—An siRNA-p24-resistant p24 cDNA was created by changing six nucleotides in the target sequence of siRNA-p24 that have no effect on amino acid sequence (CCGAATAGCAATCCCAGAC; underlined letters indicate replaced nucleotides). Because the target sequence for siRNA-p150 is in the 3′-UTR, we used a p150 cDNA 3′-UTR truncation (a gift of Dr. M. Katsuno and G. Sobue (12)) to generate a siRNA-p150-resistant p150 cDNA. To generate a pantropic retrovirus, HEK 293 cells were co-transfected with three plasmids: pHIT60 expressing murine leukemia virus gag pol (a gift of Dr. A. J. Kingsman (13)), pHCMV-G for vesicular stomatitis virus enveloped pseudotypes (a gift of Dr. T. Friedmann (14)), and pMSCV (Clontech) driving expression of siRNA-resistant p24 or p150 cDNA and IRES-EGFP[2] (15).

Analysis of mRNA and Protein Expression—Real-time quantitative RT-PCR was performed as described previously (16) using primer sets (p24 (forward, 5′-GAGTACATCGACCGCATTGCCATAC-3′ and reverse, 5′-TGATGTGAGCACTGTCCAGCATGG-3′) and p150^{Glued} (forward, 5′-TGCAGGCCACGCTACACCGCTATG-3′ and reverse, 5′-GCAATATCTGTAGCCTCCTGCCCAC-3′)). Immunostaining and image analyses were performed as described (11, 17). Signal specificity was tested by adding antigen for each antibody into the blocking solution. Relative fluorescence intensity was measured using ImageJ software. Immunoprecipitation and immunoblot analyses were performed according to standard procedures (18).

TUNEL—TUNEL assays were performed using the Fluorometric TUNEL assay kit (Promega, Madison, WI). Briefly, cells fixed with paraformaldehyde and ethanol were incubated with fluorescein-dUTP and terminal deoxynucleotidyl transferase for one hour at 37 °C. Cells were propidium iodide-stained immediately prior to flow cytometry analysis (FACSCalibur, BD Biosciences).

Fluorescence in Situ Hybridization (FISH)—HeLa cells cultured on coverglass slips were fixed with 3.7% formaldehyde, denatured on a heat block, and used directly for FISH analysis using a Myc probe complementary to chromosome band 8q24 (Dako, Glostrup, Denmark) according to the manufacturer's protocol.

Reagents—Rabbit anti-p24 polyclonal antibodies were raised against a GST-p24(N) (amino acids 5–36) or a GST-p24(C) polypeptide (amino acids 145–186) and then affinity purified according to standard procedures (18). Commercial antibodies were purchased from the following suppliers: p150^{Glued} from BD Biosciences; actin (product no. 1378 996) from Roche Diagnostics; and α-tubulin (product no. T9026) and γ-tubulin (product no. T6557) from Sigma. Hoechst 33342 was purchased from Invitrogen.

[2] The abbreviations used are: EGFP, enhanced GFP; FISH, fluorescence in situ hybridization; IRES, internal ribosomal entry site.

RESULTS

Down-regulation of p24 and p150^{Glued} Using siRNA—We initially used HeLa(tc) cells, a HeLa subline that allows high efficiency siRNA transfection (typically >90%) (11), for siRNA transfections. HeLa(tc) cells treated with siRNA (100 nM for 24 h) specific for p24 (siRNA-p24) or p150^{Glued} (siRNA-p150) showed a 5-fold approximate decrease in mRNA expression levels relative to cells treated with scrambled control siRNA (control siRNA) (Fig. 1*A*).

We used rabbits to generate two polyclonal antibodies, p24(N) and p24(C), against different portions of p24 (see "Experimental Procedures"). Both antibodies recognized an endogenous p24 protein (Fig. 1*B*, *lane 1*) that migrated to the same position in SDS-polyacrylamide gels as exogenous p24 protein expressed from a eukaryote plasmid expression vector (*lane 4*). As previously reported, the apparent mass of p24 is ~21 kDa, slightly smaller than the mass predicted from the amino acid sequence (4). Cells treated with siRNA-p24 (100 nM) for 48 h expressed 10-fold lower levels of p24 protein relative to untreated cells or cells treated with control siRNA (*lane 3*). Immunoblot analysis using p150^{Glued} antibody revealed a 20-fold reduction in p150^{Glued} protein levels in cells treated with siRNA-p150 for 72 h (Fig. 1*C*).

Similar to previous reports (4), immunostaining of mitotic cells with p24(C) antibody showed p24 localized to kinetochores and centrosomes in prometaphase and metaphase cells with considerable signal remaining in early anaphase (Fig. 1*D*). Although the general localization of p150^{Glued} (Fig. 1*E*) overlaps with p24, some specific differences were distinguished in cells doubly stained with p24 and p150^{Glued} antibodies (Fig. 1*F*). First, staining of mitotic spindles with anti-p150 was strong, whereas only weak fluorescence was detected with anti-p24. Second, although both p24 and p150 signals were detected at prometaphase kinetochores, p150 signal intensity diminished rapidly in metaphase, whereas p24 signals were remained until anaphase. The contrast between the intense p24 immunofluorescence maintained in anaphase centrosomes with diminished p150^{Glued} immunofluorescence that is barely detectable in early anaphase suggests a rapid efflux of p150^{Glued} from centrosomes during metaphase.

When cells were transfected with Cy3-labeled siRNA-p24, the intensity of p24 immunofluorescence in Cy3 staining-positive cells was reduced (Fig. 1*G*, *left panels*). p150^{Glued} signals were also reduced in response to treatment with siRNA-p150 (100 nM) for 72 h (*right panels*).

siRNA-p24 or -p150 Induces Mitotic Disturbances—Although we observed no obvious morphological differences in phase-contrast microscopy images of interphasic HeLa(tc) cells treated for up to 72 h with control siRNA, siRNA-p24, or siRNA-p150 (100 nM) (data not shown), we did observe a significant increase in the mitotic index of cells 48 h after transfection with siRNA-p24 relative to control siRNA (11.1% relative to 4%) ($p < 0.01$, Chi-square test, Fig. 2*A*). In addition,

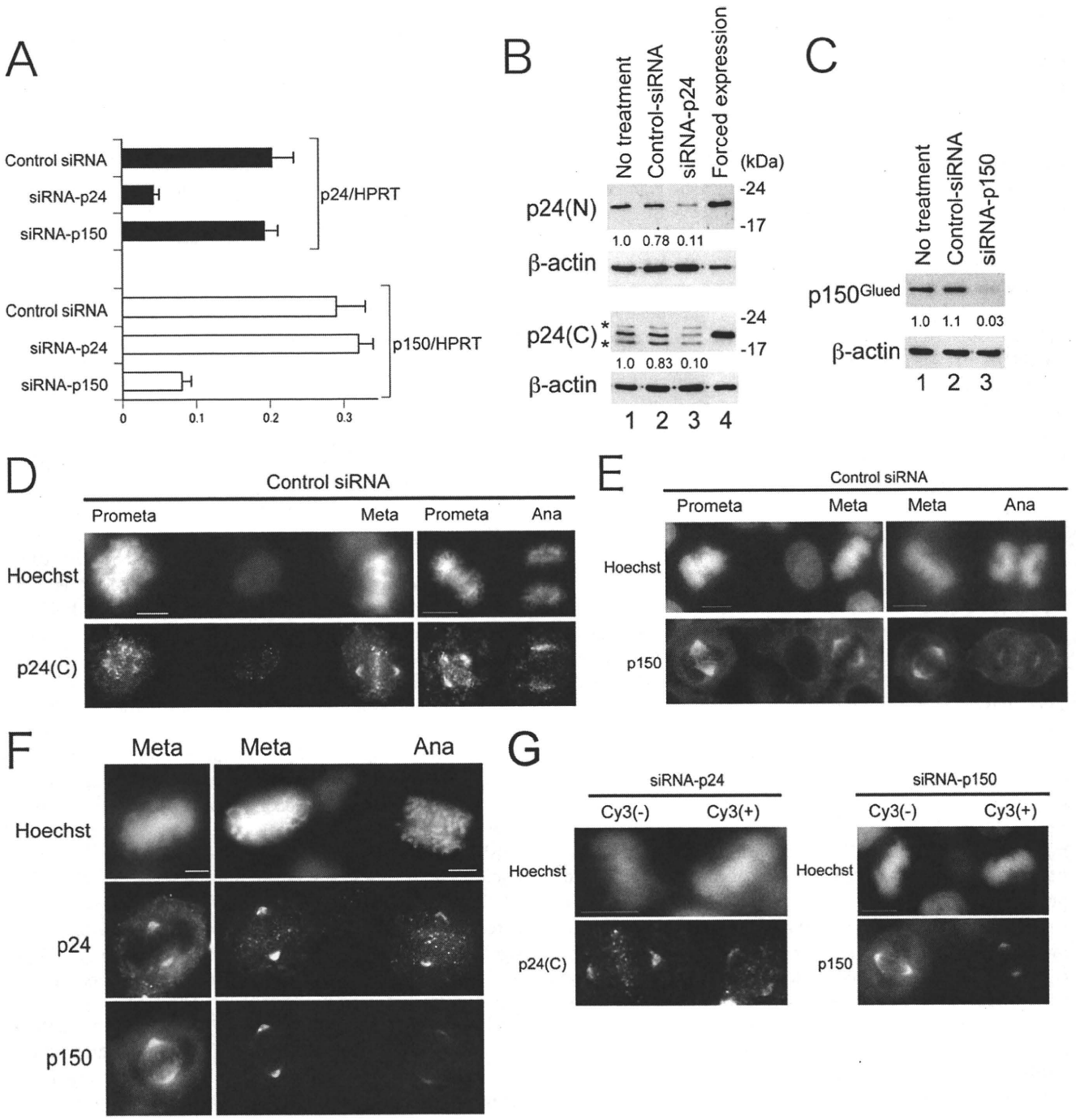

FIGURE 1. **Down-regulation of p24 and p150 by siRNA.** *A*, p24 (*black bars*) and p150^{Glued} (*open bars*) mRNA expression levels in HeLa(tc) cells treated with control siRNA, siRNA-p24, or siRNA-p150 (100 nM) for 24 h. Real-time quantitative PCR data were normalized against hypoxanthine phosphoribosyl transferase (*HPRT*), and the mean and S.D. for three independent experiments is represented. *B*, immunoblot analysis using p24(N), p24(C), or β-actin antibody. *Lane 1*, untreated HeLa(tc) cells; *lane 2*, cells treated with control siRNA (100 nM) for 48 h; *lane 3*, cells treated with siRNA-p24 (100 nM) for 48 h; *lane 4*, HEK 293 cells transfected with pcDNA3-p24, a eukaryotic expression vector. Ratios of relative intensity (p24/actin) measured by densitometry are indicated below each lane. *Asterisks* indicate cross-reactive bands appearing in HeLa but not HEK 293 cells. *C*, immunoblot analysis using p150^{Glued} or β-actin antibody. *Lane 1*, untreated HeLa(tc) cells; *lane 2*, cells treated with control siRNA (100 nM) for 72 h; *lane 3*, cells treated with siRNA-p150 (100 nM) for 72 h. Ratios of relative intensity (p150/actin) measured by densitometry are shown below. *D–G*, immunostaining of mitotic HeLa cells treated with siRNA indicated *above* with antibodies indicated on the *left*. DNA was stained with Hoechst 33342, and the mitotic phase of cells are labeled above. *Bars*, 10 μm (*D*, *E*, and *G*) and 5 μm (*F*). *Meta*, metaphase; *Ana*, anaphase; *Prometa*, prometaphase.

there was also a significant increase ($p < 0.01$) in the number of dead cells (determined by trypan blue dye exclusion) among the cells treated with siRNA-p24 for 48 and 72 h (7.2%, 15/207 and 17.1% 36/211, respectively) and siRNA-p150 for 72 h (8.0%, 16/202) relative to untreated cells (2.0%, 8/401).

Flow cytometric analyses of HeLa cells treated with siRNA-p24 for 48 h and stained with propidium iodide dem-

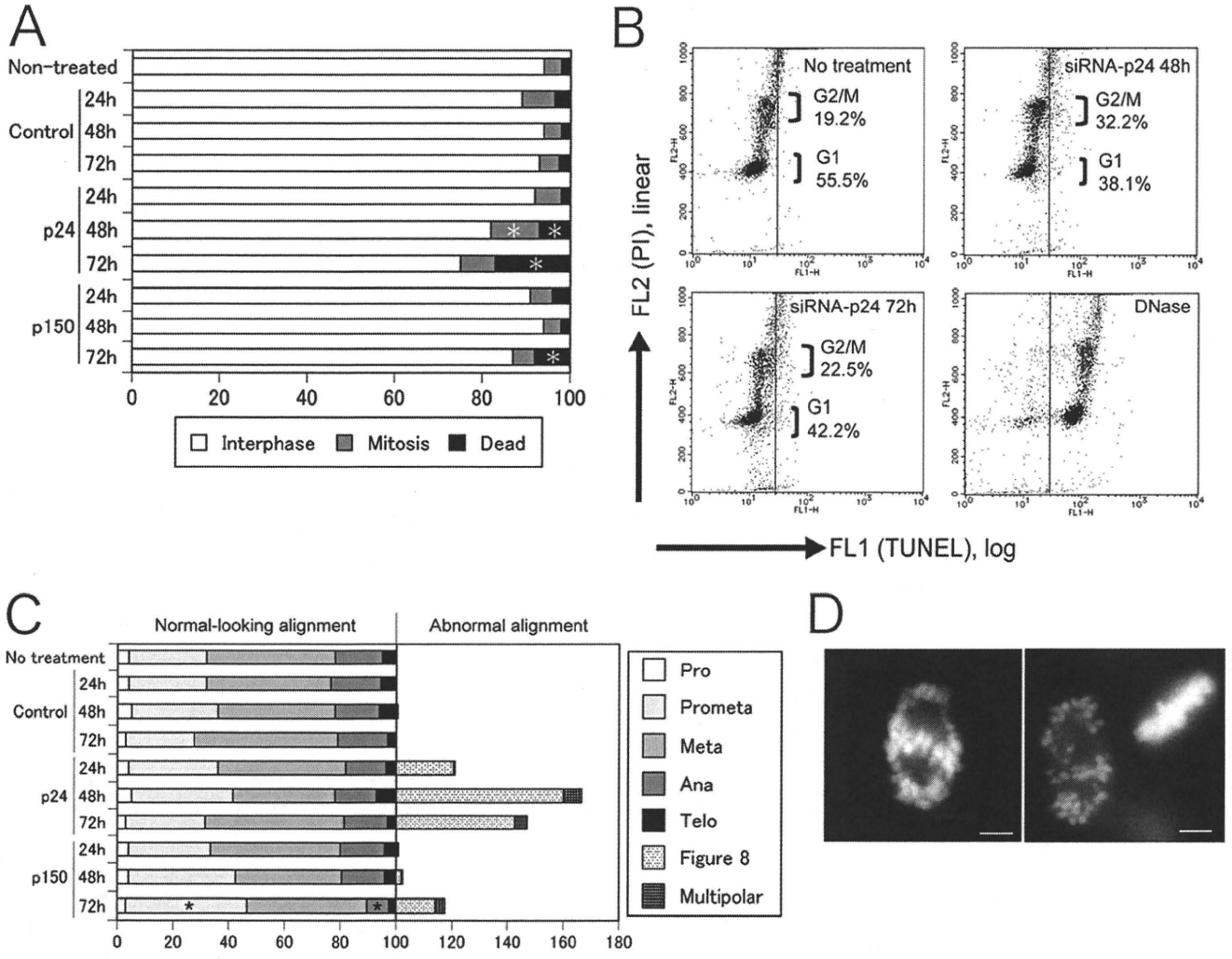

FIGURE 2. **Down-regulation of p24 and p150 induces mitotic abnormalities in HeLa(tc) cells.** *A*, cells were treated with each siRNA for periods indicated on the *left*. From a total of 300 cells counted/treatment, the relative percentages of mitotic, interphase, and dead cells determined by separation of floating cells (mitotic and dead *versus* interphase) and by trypan blue dye exclusion (live *versus* dead) are indicated by *shading*. *Asterisks* indicate a statistically significant ($p < 0.01$) increase relative to the no treatment control using Chi-square test. *B*, cells treated with siRNA-p24 for indicated periods were stained with propidium iodide (*PI*) just prior to flow cytometry and TUNEL analysis. FL1 values on the *horizontal axis* indicate the amount of dUTP polymerized by DNA free 3′ ends, whereas FL2 values on the *vertical axis* show the DNA content. *C*, from a total of 300 cells counted/treatment, the percentages of mitotic cells with normal-looking chromosome alignment (100% total) or abnormal mitosis were determined from observations of Hoechst 33342-stained nuclei. *Asterisks* indicate statistically significant changes in a particular mitotic phase ($p < 0.01$) relative to the no treatment control by Chi-square test. *D*, representative images of Hoescht 33342-stained chromosomes in a figure eight alignment. *Bar*, 5 μm. *Pro*, prophase; *Prometa*, prometaphase; *Meta*, metaphase; *Ana*, anaphase; *Telo*, telophase.

onstrate that siRNA-p24 induces mitotic delay/arrest, in that the G_2/M-phase ratio (Fig. 2*B*, *vertical axis*) was significantly higher in treated cells (32.2%) than in cells without treatment (19.2%) However, the cell death induced by siRNA-p24 does not appear apoptotic because TUNEL assays showed only a small increase in DNA free 3′ ends (Fig. 2*B*, *horizontal axis*; see DNase-treated HeLa cell panel as a positive control) in siRNA-p24-treated cells.

To determine the effects of down-regulation of p24 and $p150^{Glued}$ on mitosis, we analyzed chromosome alignment in Hoechst 33342-stained mitotic cells. Although treatment of cells with control siRNA (100 nM) for up to 72 h did not affect their distribution (Fig. 2*C*), we observed that treatment with siRNA-p24 for 48 h specifically induced one of two distinct patterns of abnormal chromosome alignment in 39.8% (133/334) of mitotic cells (Fig. 2*C*). First, chromosomes in 120 mitotic cells treated with siRNA-p24 for 48 h aligned abnormally to resemble a figure eight pattern (Fig. 2*D*), whereas the same pattern almost never appeared (<1/200) in mitotic cells without siRNA treatment or those treated with control siRNA. Second, 3.9% (13/334) of mitotic cells treated with siRNA-p24 for 48 h demonstrated multipolar mitoses. Among the remaining 201 mitotic cells with normal-looking chromosome alignment, the distribution of cells in each mitotic phase was not altered. Relative to cells treated for 48 h, cells treated with siRNA-p24 for 24 or 72 h showed the same abnormal pattern of chromosome alignment but at a lower frequency (Fig. 2*C*).

In contrast to siRNA-p24-treated cells, cells treated with siRNA-p150 for 48 h showed no significant change in distribution among mitotic phases, and only a few cells demon-

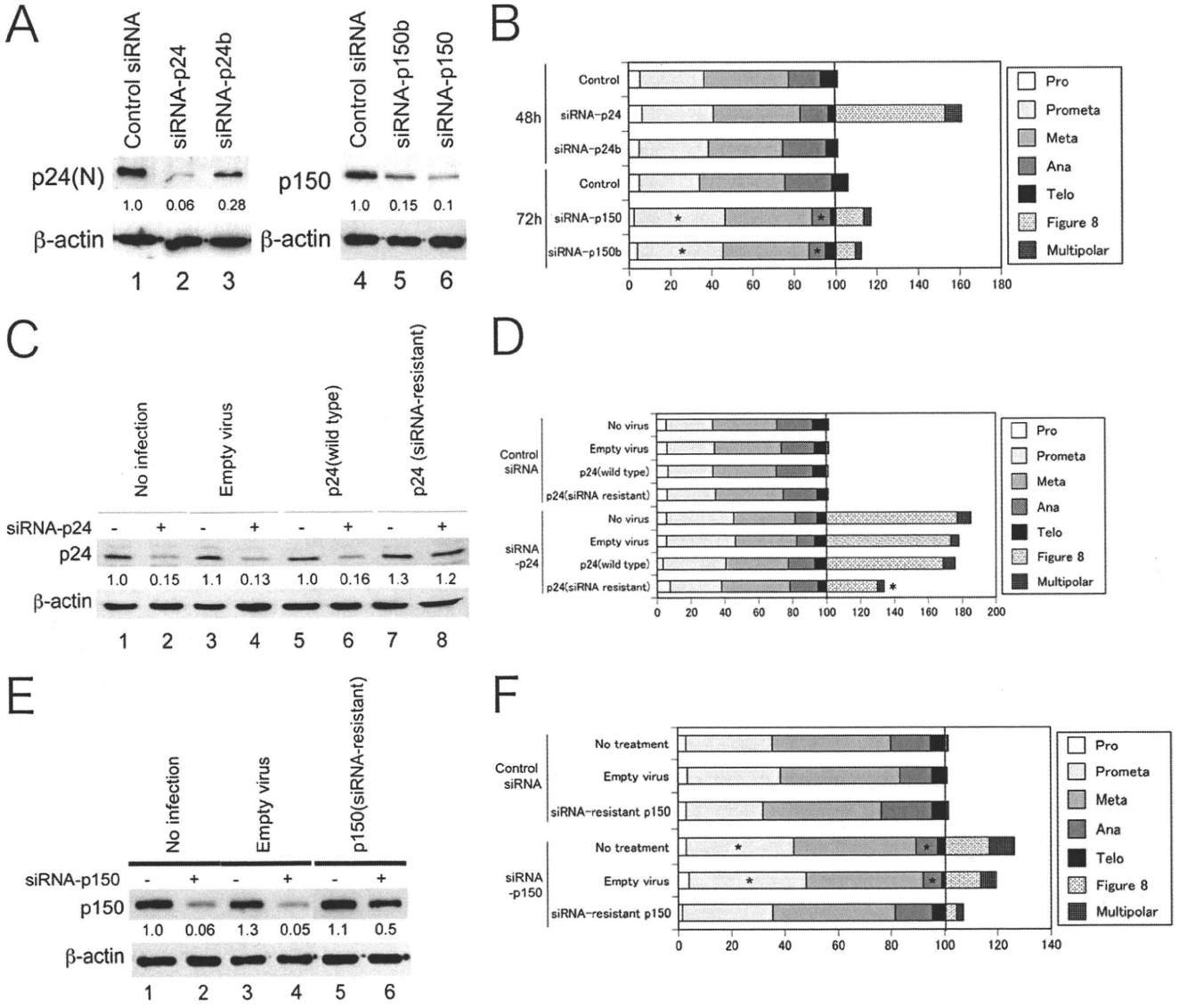

FIGURE 3. *A*, immunoblot analysis using p24(N), p150, or β-actin antibody. HeLa(tc) cells were treated with the siRNA (100 nM) indicated above for 48 (*lanes 1–3*) or 72 h (*lanes 4–6*). Ratios of signal intensity relative to actin (measured using densitometry) are indicated *below each lane*. *B*, *D*, and *F*, the percentages of mitotic cells with normal-looking chromosome alignment (100% total) or abnormal mitosis were determined from observations of Hoechst 33342-stained nuclei in a total of 300 cells/treatment. *Asterisks* indicate statistically significant changes in a particular mitotic phase ($p < 0.01$) relative to the no treatment control using the Chi-square test. *C*, immunoblot analyses using p24(N) or β-actin antibody. *Lanes 1* and *2*, uninfected HeLa(tc) cells; *lanes 3* and *4*, cells infected with empty virus; *lanes 5* and *6*, cells infected with virus containing wild type p24 cDNA; *lanes 7* and *8*, cells infected with virus containing siRNA-resistant p24 cDNA. *Lanes 1*, *3*, *5*, and *7*, cells were treated with control siRNA; *lanes 2*, *4*, *6*, and *8*, cells were treated with siRNA-p24 (100 nM) for 48 h. Ratios of relative signal intensity (p24/actin) are indicated *below each lane*. *E*, immunoblot analysis using p150 or β-actin antibody. *Lanes 1* and *2*, uninfected HeLa(tc) cells; *lanes 3* and *4*, cells infected with empty virus; *lanes 5* and *6*, cells infected with virus containing siRNA-resistant p150 cDNA. *Lanes 1*, *3*, and *5*, cells were treated with control siRNA; *lanes 2*, *4*, and *6*, cells were treated with siRNA-p150 (100 nM) for 72 h. Ratios of relative intensity (p150/actin) are indicated *below each lane*. *Pro*, prophase; *Prometa*, prometaphase; *Meta*, metaphase; *Ana*, anaphase; *Telo*, telophase.

strated the figure eight chromosome alignment seen with siRNA-p24 (Fig. 2*C*). After an additional 24 h of treatment with siRNA-p150, however, we observed a significant increase in the ratio of prometaphase cells and a corresponding decrease in anaphase and telophase cells. In addition, small percentages of mitotic cells showed the figure eight chromosomal alignment (11.9%, 28/236) or multipolar mitoses (3.0%, 7/236).

We also treated cells with secondary siRNAs that target alternative sequences in the p24 or $p150^{Glued}$ genes. When cells were treated with siRNA-p24b, which only reduced p24 levels ~3-fold (Fig. 3*A*), few mitotic cells showed the figure eight chromosome alignment (Fig. 3*B*), suggesting that greater reductions in p24 protein levels are required to induce the figure eight alignment. In contrast, cells treated with siRNA-p150b reduced p150 to levels similar to siRNA-p150 (Fig. 3*A*) and showed similar mitotic disturbances, including an increased ratio of prometaphase cells, a decreased ratio of anaphase/telophase cells, and a few cells with figure eight chromosome alignment.

To exclude the possibility that the figure eight chromosome alignment is an off-target effect of siRNA-p24, we performed

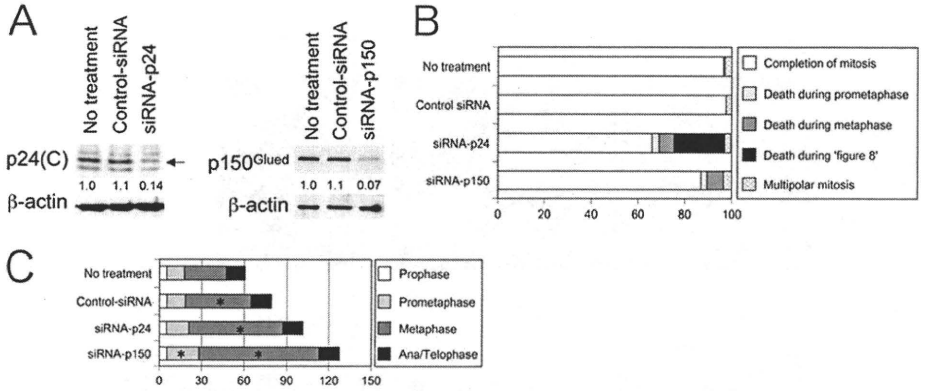

FIGURE 4. **Time-lapse observations of mitotic cells.** *A*, immunoblot analyses of lysates from U2OS cells using p24(C), p150^{Glued}, or β-actin antibody. Cells were treated with the siRNA indicated for 72 h. Ratios of relative intensity (p24 or p150/actin) measured by densitometry are indicated *below each lane*. An *arrow* marks the position of p24. *B*, U2OS cells expressing an H2B-GFP fusion protein were treated with control siRNA or siRNA-p150 for >48 h or with siRNA-p24 for >24 h. Percentages of cells demonstrating termination of mitosis in one of the manners listed on the *right* are indicated with *shading*. *C*, the average duration of each mitotic phase (min) in cells that completed mitosis are indicated by shading. *Asterisks* indicate a statistically significant increase in duration ($p < 0.05$) relative to the no treatment control.

rescue experiments by expressing a siRNA-p24-resistant p24 mRNA from a pantropic retrovirus containing EGFP as a selection marker (see "Experimental Procedures"). EGFP-positive cells were sorted using flow cytometry and then treated with siRNA-p24.

Immunoblot analyses revealed similar levels of p24 in cells infected with retrovirus containing p24 cDNA or siRNA-resistant p24 cDNA (Fig. 3*C*, *lanes 5* and *7*). Following treatment with siRNA-p24 (100 nM for 48 h), uninfected cells, as well as those infected with empty virus or virus containing wild-type cDNA (Fig. 3*C*, *lanes 2*, *4*, and *6*) showed down-regulation of p24 protein. In contrast, there was no significant reduction in p24 levels in cells expressing the siRNA-resistant p24 cDNA (Fig. 3*C*, *lane 8*). Mitotic cells with the figure eight chromosome alignment were observed in cells infected with empty virus (73%) or virus containing wild type cDNA (68.5%) at virtually the same frequency as uninfected cells (77.3%) (Fig. 3*D*). Only cells infected with virus containing the siRNA-resistant cDNA showed a significant reduction in the frequency figure eight mitoses (34.5%, $p < 0.01$), suggesting that p24 is indeed effective in preventing chromosomes from the figure eight alignment.

We also expressed a siRNA-resistant p150 cDNA in HeLa cells using the same pantropic retrovirus system (Fig. 3*E*). Unlike uninfected cells or those infected with the empty virus, cells expressing siRNA-resistant cDNA showed little decrease in p150 levels following siRNA treatment. Similarly, there was no significant increase in prometaphase or decrease in ana/telophase ratios in cells treated with siRNA-p150 (Fig. 3*F*), and the ratio of cells with the figure eight chromosome alignment decreased.

Chromosomes Align into a Figure Eight after Metaphase Arrest—To further analyze the mitotic disturbances induced by p24 or p150^{Glued} down-regulation, we established a U2OS cell line expressing a histone H2B-GFP fusion protein constitutively (19), transfected these cells with control, p24, or p150^{Glued} siRNAs (efficiency typically 70%) and then collected time-lapse images of the transfected cells. In these cells, the magnitude in reduction of p24 or p150^{Glued} protein expression levels by siRNA-p24 or siRNA-p150, respectively, were similar to those achieved in HeLa cells (Fig. 4*A*).

More than 95% of mitotic cells without siRNA treatment or treated with control siRNA completed mitosis (Fig. 4*B*, also see supplemental Movie 1). Cells treated with control siRNA demonstrated a significant elongation of metaphase (46 min in control siRNA-treated cells to compare with 29 min in untreated cells, $p < 0.05$), whereas the durations of prophase, prometaphase, and anaphase and telophase combined (ana/telophase) were not affected (Fig. 4*C*). These data suggest that U2OS cells treated with scrambled siRNA and/or cationic liposome experience a delayed progression through metaphase. Only one of 180 (0.55%) untreated cells and zero of 156 cells treated with control siRNA died while in mitosis.

When cells were treated with siRNA-p24 (100 nM) for >24 h, we observed a significant delay in metaphase (average of 66 min) relative to control siRNA-treated cells (average of 46 min, $p < 0.05$, Fig. 4*C*). There was no elongation in the duration of prometaphase or ana/telophase. We also observed cell death more frequently in siRNA-p24-treated cells: 3% (10/333) or 6.5% (22/333) of mitotic cells underwent cell death during prometaphase or metaphase, respectively (Fig. 4*B*). Intriguingly, in 21.5% (72/333) of siRNA-p24-treated mitotic cells, chromosomes aligned at the metaphase plate during prolonged metaphase broke up into a figure eight pattern (supplemental Movie 2). This similarity to the abnormal chromosome alignment observed in siRNA-p24-treated HeLa cells (Fig. 2*D*) indicates that these are not prometaphase cells but rather post-metaphasic cells that fail to enter anaphase. All 72 cells with figure eight chromosome alignment underwent cell death eventually (an average of 164 min after breakup of chromosome alignment at the metaphase plate) (supplemental Movie 2). Overall, 31% (104/333) of siRNA-p24-treated mitotic cells underwent cell death, whereas these cells in interphase rarely underwent apoptosis (< 0.1%).

In contrast to control siRNA- or siRNA-p24-treated cells, cells treated with siRNA-p150 for >48 h demonstrated delayed prometaphase (average of 23 min to compare with 12 min in control siRNA-treated cells, $p < 0.05$, Fig. 4*C*), during

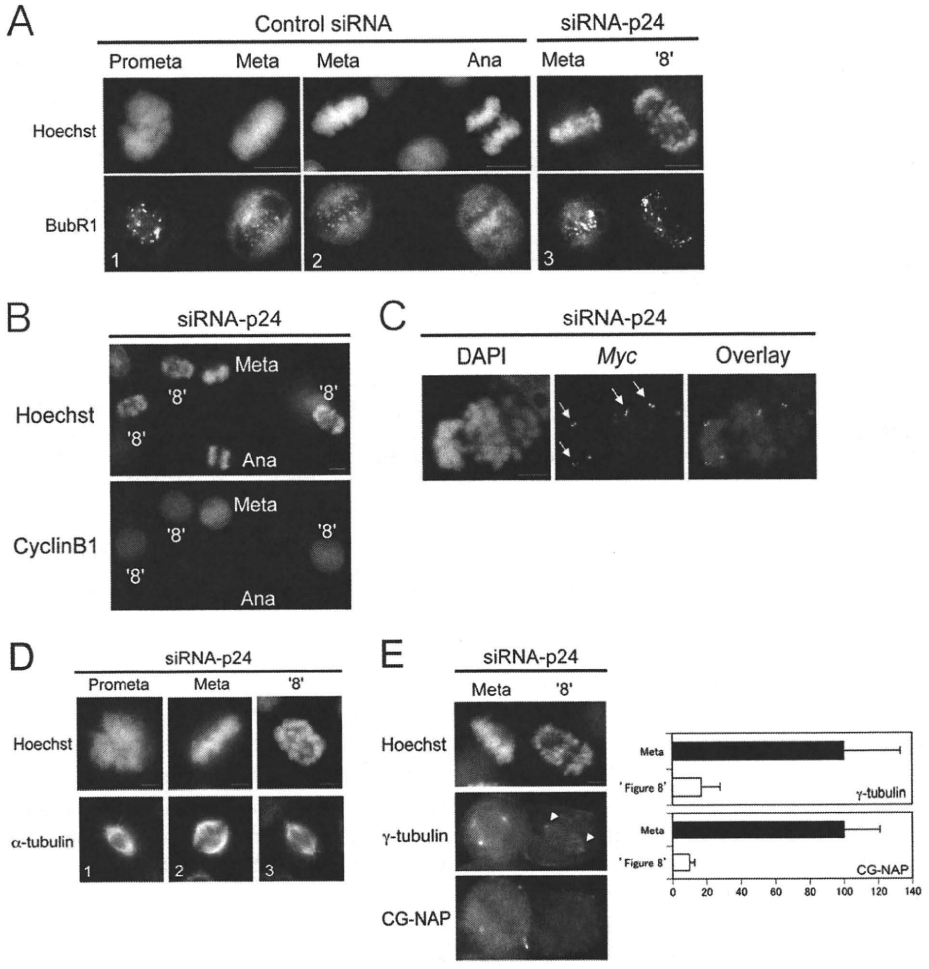

FIGURE 5. **Mechanisms of figure eight chromosome alignment.** *A*, *B*, and *D*, HeLa cells were treated with the siRNA indicated and immunostained with the antibody indicated on the *left*. DNA was stained with Hoechst 33342, and the mitotic phase of cells are labeled *above or within* each image. *Bars*, 10 μm (*A* and *B*) and 5 μm (*D*). *C*, HeLa cells treated with siRNA-p24 were fixed with formaldehyde, denatured, and hybridized with a c-*myc* probe for FISH analysis. DNA was stained with DAPI. *Arrows* mark pairs of dots that indicate sister chromatids. *Bar*, 5 μm. *E*, HeLa cells were treated with siRNA-p24 and immunostained with the antibody indicated on the *left*. Relative fluorescence intensity of proteins in either metaphase (*black bars*) or figure eight (*open bars*) centrosomes (*right panels*). The mean (+ S.D.) intensity of 50 centrosomal areas was measured, and background levels were subtracted. *Bar*, 5 μm. *Prometa*, prometaphase; *Meta*, metaphase; *Ana*, anaphase.

which 2.4% (4/163) underwent cell death. Moreover, the metaphase delay induced by siRNA-p150 (average 85 min, Fig. 4*C*, see Video 3) was more severe than in cells treated with siRNA-p24 and 6.7% (11/163) of siRNA-p150-treated mitotic cells underwent cell death during metaphase. These findings are consistent with previous experiments in which HeLa cells treated with siRNA-p150 showed increased ratios of cells in prometaphase and metaphase relative to cells in anaphase and telophase (Fig. 2*C*). Unlike cells treated with siRNA-p24, none of these mitotic cells showed chromosomes aligned in a figure eight pattern, and all cells that survived through prometaphase and metaphase entered anaphase.

Cells with Figure Eight Chromosome Alignment Share Features with Prometaphase—Our findings demonstrate that down-regulation of either p24 or $p150^{Glued}$ induces severe metaphasic delays. This phenotype is analogous to a previous report about cells that undergo metaphase arrest/delay when dynactin is depleted by dynamitin overexpression (8). In that case, the delay is most likely due to a defect in the function of the dynein-dynactin complex, which removes spindle checkpoint proteins such as BubR1 from kinetochores during metaphase (reviewed in Ref. 20). Indeed, when cells were treated with control siRNA, BubR1 signals localized to kinetochores in prometaphase (Fig. 5*A*, *panel 1*), after which the signal decreased rapidly during metaphase and anaphase (*panels 1* and *2*). In contrast, cells treated with siRNA-p24 showed the same intensity of BubR1 immunofluorescence at the kinetochores of metaphase chromosomes as that in prometaphase cells, including those cells with a figure eight chromosome alignment (*panel 3*).

Despite their similarities in appearance to prometaphase (rather than anaphase) cells, the figure eight chromosome alignment is only seen in cells that have progressed through metaphase (supplemental Movie 2). To further characterize the timing of this unique chromosomal alignment, we looked at expression of cyclin B1, a molecule that is present during metaphase (Fig. 5*B*, *Meta*) and then degraded rapidly in anaphase (*Ana*). We observed positive cyclin B1 immunofluorescence in all mitotic cells with a figure eight chromosome alignment. Moreover, FISH images of the c-*myc* gene on

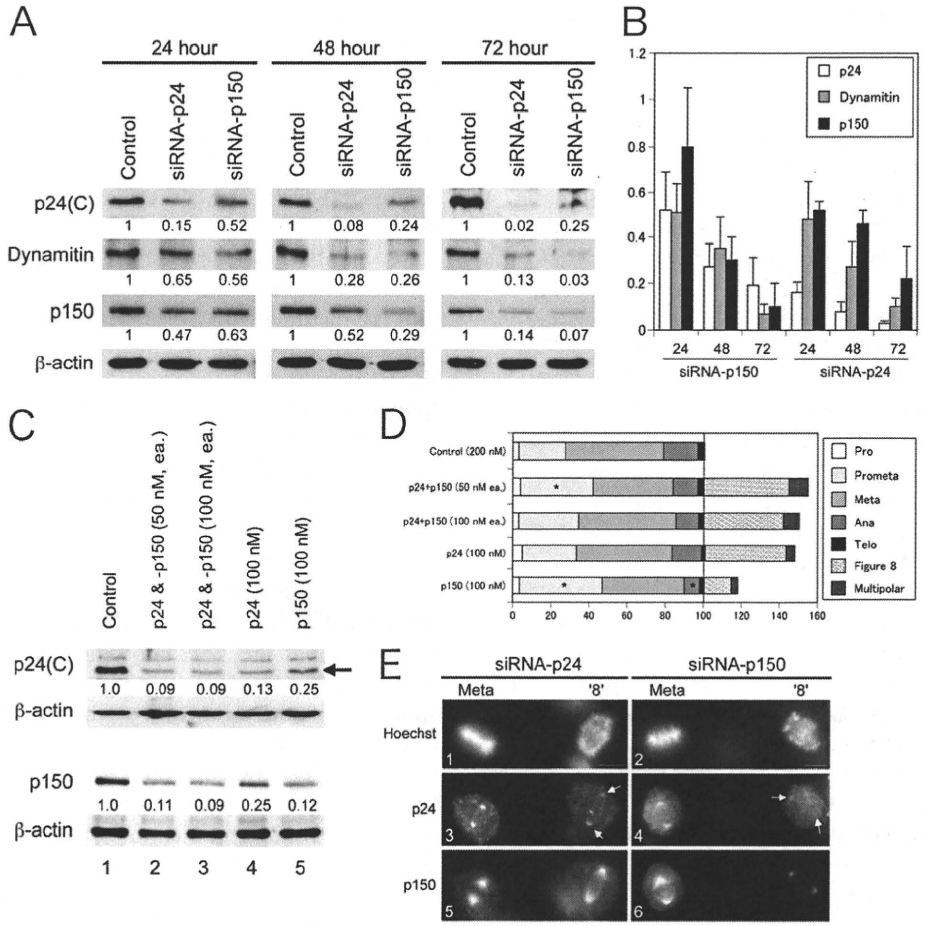

FIGURE 6. **p24 expression levels relate to figure eight configuration.** *A* and *C*, immunoblot analyses using p24(C), dynamitin, p150^{Glued}, or β-actin antibody. HeLa cells were treated with siRNA (100 nM, otherwise indicated) as indicated above for 72 h. Ratios of relative intensity (p24, dynamitin, or p150 actin) measured by densitometry are indicated *below each lane*. Data are representative of four independent experiments that yielded similar results. *B*, average and S.D. protein expression levels in four independent experiments of p24, dynamitin, and p150^{Glued} relative to control siRNA-treated cells. *D*, HeLa (tc) cells were treated with the siRNA indicated on the *left* for 72 h. From a total of 300 cells counted/treatment, the percentages of mitotic cells with normal-looking chromosome alignment (100% total) or abnormal mitosis were determined from observations of Hoechst 33342-stained nuclei. *Asterisks* indicate statistically significant changes in a particular mitotic phase ($p < 0.01$) relative to the no treatment control using a Chi-square test. *E*, HeLa cells were treated with the siRNA indicated above and immunostained with the antibody indicated on the *left*. DNA was stained with Hoechst 33342, and the mitotic phase of each cell is labeled *above*. *Bar*, 10 μm. *Pro*, prophase; *Prometa*, prometaphase; *Meta*, metaphase; *Ana*, anaphase; *Telo*, telophase. '*8*', figure eight.

chromosome band 8q24 indicate that sister chromatids in cells with figure eight alignment have yet to segregate because four pairs of dots are visible on chromosomes in figure eight cells (Fig. 5*C*, *arrows*; FISH with chromosome 8-specific centromeric probes revealed that HeLa(tc) cells have four chromosome 8 (data not shown)). These data suggest that cells with figure eight chromosome alignment are most like prometaphase cells.

Because the alignment of chromosomes on the metaphase plate is mediated by tension between the spindle poles, reversal of the mitotic process by siRNA-p24 interference may be due to reductions in spindle tension. Using α-tubulin immunostaining, we compared the density and morphology of spindles in cells at different stages of mitosis. In cells displaying a figure eight configuration (Fig. 5*D*, *panel 3*), the robust fluorescence characteristic of metaphase mitotic spindles (*panel 2*) reverted to a shape and intensity more characteristic of mitotic spindles in prometaphase (*panel 1*). Moreover, the marked decrease in immunostaining signal intensity for γ-tubulin and CG-NAP (pivotal components of the γ-tubulin ring complex that provides microtubule nucleation sites) in figure eight-stage cells relative to metaphase cells (Fig. 5*E*) suggests that p24 is required to maintain the integrity of metaphase centrosomes.

p24 Levels Relate to Figure Eight Chromosome Alignment—In parallel experiments conducted in two different cell lines (HeLa or U2OS), metaphase arrest/delay was induced similarly following treatment with either siRNA-p24 or siRNA-p150; however, siRNA-p24 was significantly more effective than siRNA-p150 in inducing the figure eight chromosome alignment during metaphase (Figs. 2*C* and 4, *B* and *C*). We did not observe any change in expression of p150^{Glued} and p24 mRNAs following treatment with siRNA-p24 or siRNA-p150, respectively (Fig. 1*A*). However, both of these siRNAs did reduce protein expression levels of p24, p150^{Glued}, and dynamitin in HeLa(tc) cells (Fig. 6*A*). Similar results were obtained in U2OS cells (data not shown). Similar to previous reports demonstrating that overexpression of dynamitin disrupts dynactin structure (2), our results with p24 and p150^{Glued} suggest that balanced availability of all

components is required to maintain the stability of the dynactin complex.

To test whether changes in p24 expression levels are sufficient to induce the figure eight chromosome alignment, we treated cells with siRNAs and then measured the expression levels of dynactin components and observed alterations in chromosome alignment. When cells were treated with siRNA-p150 for 24 or 48 h, expression levels of p24, dynamitin, and $p150^{Glued}$ relative to control cells were ~25% or higher (Fig. 6*B*), but no mitotic abnormalities were observed (Fig. 2, *A* and *C*). Treatment with siRNA-p150 for 72 h reduced the expression levels of dynamitin and $p150^{Glued}$ to <10% and p24 to ~20%, and this treatment induced metaphase arrest/delay and a few cells with the figure eight chromosome alignment (Fig. 2*C*). In contrast, treatment of cells with siRNA-p24 for 24 or 48 h reduced the expression levels of p24 to less than 15%, while maintaining relatively high (>25%) levels of dynamitin and $p150^{Glued}$. In this case, more mitotic cells showed a figure eight chromosome alignment (Fig. 2*C*).

We also treated HeLa(tc) cells with a combination of both siRNA-p24 and siRNA-p150 (50 or 100 nM each) for 72 h. Although this procedure reduced both p24 and p150 expression levels to ~10% of those in control cells (Fig. 6*C*, *lanes 2* and *3*), the ratio of cells in the figure eight alignment (42–45%) was virtually the same as cells treated with siRNA-p24 alone (43%, Fig. 6*D*), in which p24 and p150 expression are reduced to ~10 and 25% of control cells, respectively (Fig. 6*C*, *lane 4*). Once again, cells treated with siRNA-p150 alone that expressed p24 at 25% and p150 at 10% of control cells (*lane 5*) showed only a small number (~10%) of mitotic cells with the figure eight configuration (Fig. 6*D*). These data demonstrate that among all components of the dynactin complex, manipulation of p24 expression levels is most likely to result in cells assuming the figure eight configuration.

Further evidence in support of this correlation was observed when treated cells were immunostained simultaneously for p24 and $p150^{Glued}$. p24 immunofluorescence at centrosomes of mitotic HeLa(tc) cells treated with siRNA-p24 was markedly less intense in cells with the figure eight chromosome alignment relative to metaphasic cells in the same microscopic field (Fig. 6*E*, *panel 3*). Intriguingly, p150 immunofluorescence at centrosomes in most (23/25) of these figure eight cells was as bright as the signal in metaphasic cells (Fig. 6*E*, *panel 5*). In contrast, in cells treated with siRNA-p150, both p24 and p150 immunofluorescence signals in figure eight cells were markedly reduced (Fig. 6*E*, *panels 4* and *6*) in all cells observed (25/25). These results suggest that failure of p24 to accumulate in mitotic centrosomes induces figure eight chromosome alignment.

DISCUSSION

In this report, we treated HeLa and U2OS cells with siRNAs specific for p24 or $p150^{Glued}$, two components of the projecting arm of the dynactin complex. Time-lapse observations reveal that treatment of siRNA-p24 induces severe metaphase delay. In >40% of metaphase cells struggling to enter anaphase, chromosomes aligned on the metaphase plate break away and assume a configuration resembling a figure eight. In time, all cells with the figure eight alignment die without completing mitosis. In contrast with p24, cells treated with siRNA-p150 demonstrate severe delays in metaphase, but most cells do not assume the figure eight alignment and ultimately progress to anaphase. Neither p24 nor $p150^{Glued}$ appears to be involved in the progression of anaphase and telophase.

Reductions in p24 or $p150^{Glued}$ protein levels induce metaphase arrest/delay (Fig. 4*C* and supplemental Movies 1–3). This is consistent with a previous report in which cells overexpress dynamitin, which down-regulates dynactin function, also undergo metaphase arrest/delay (8). Failure to remove spindle checkpoint proteins such as BubR1 from kinetochores (Fig. 5*A*) results in metaphase delay because checkpoint proteins inhibit cdc20, a specific activator of the anaphase-promoting complex/cyclosome (reviewed in Ref. 20). Because anaphase-promoting complex/cyclosome functions as an E3 ubiquitin ligase, mitotic checkpoint proteins that are remain on kinetochores delay ubiquitin-dependent degradation of cyclin B1 (Fig. 5*B*) or securin, which then inhibits cohesin hydrolysis and blocks chromosome segregation (Fig. 5*C*).

Nonetheless, the transition of chromosomes from a metaphase to a figure eight configuration does not appear to be a direct result of spindle checkpoint protein retention at kinetochores. Because there is a marked reduction of γ-tubulin and CG-NAP signals at mitotic centrosomes in cells with the figure eight chromosome alignment (Fig. 5*E*), insufficient amounts of γ-TuRC in metaphase centrosomes appear to be one of the major factors driving the phenotype. Thus, we hypothesize that loss of spindle microtubule tension (Fig. 5*D*) is the defect that induces chromosomes to break away from alignment at the metaphase plate.

The two functions of the dynactin complex are to remove spindle checkpoint proteins from kinetochores and to maintain centrosome integrity until entry into anaphase. Although we have observed that neither of these functions are disturbed when expression levels of p24, dynamitin, or $p150^{Glued}$ remain at least 25% of control levels (siRNA-p150 for 48 h, see Figs. 2*C* and 6*A*), we did note that a 10-fold reduction in the expression of either p24 or $p150^{Glued}$ impaired the removal of checkpoint proteins, resulting in metaphase delay. In contrast, chromosome integrity and the resulting formation of figure eight cells was only induced with a 10-fold reduction in p24 levels but not with a reduction in $p150^{Glued}$. Immunofluorescence experiments also emphasized a correlation between accumulation of p24 (but not $p150^{Glued}$) in centrosomes and figure eight chromosome alignment (Fig. 6*E*). These data suggest that p24 acts independently of $p150^{Glued}$ in metaphase centrosomes, where it helps maintain chromosome integrity and prevents breakaway until entry into anaphase.

Although it is generally accepted that p24, dynamitin, and $p150^{Glued}$ function together in the dynactin projecting arm (2), we and others (4, 21) have observed that the localization of different dynactin components during mitosis varies considerably. For example, p24 immunofluorescence is strong at centrosomes relative to mitotic spindles or kinetochores. This is particularly evident during early anaphase (Fig. 1, *E* and *F*)

when p150^{Glued} immunofluorescence is barely detectable. In conclusion, our results suggest that p24 operates independently from the dynactin complex in binding to metaphase centrosomes and maintaining their integrity. To explore this hypothesis further, we are currently investigating the function of p24 in metaphase centrosomes in greater detail.

Acknowledgments—We thank Dr. K. Kevin Pfister (University of Virginia) for kindly providing antibodies against p24, Dr. M. Katsuno and G. Sobue (Nagoya University) for providing expression vectors for p150^{Glued}, and M. Nakamura for excellent technical assistance.

REFERENCES

1. Musacchio, A., and Salmon, E. D. (2007) *Nat. Rev. Mol. Cell Biol.* **8,** 379–393
2. Schroer, T. A. (2004) *Annu. Rev. Cell Dev. Biol.* **20,** 759–779
3. Pfister, K. K., Benashski, S. E., Dillman, J. F., 3rd, Patel-King, R. S., and King, S. M. (1998) *Cell Motil Cytoskeleton* **41,** 154–167
4. Karki, S., LaMonte, B., and Holzbaur, E. L. (1998) *J. Cell Biol.* **142,** 1023–1034
5. Eckley, D. M., and Schroer, T. A. (2003) *Mol. Biol. Cell* **14,** 2645–2654
6. Amaro, I. A., Costanzo, M., Boone, C., and Huffaker, T. C. (2008) *Genetics* **178,** 703–709
7. Burkhardt, J. K., Echeverri, C. J., Nilsson, T., and Vallee, R. B. (1997) *J. Cell Biol.* **139,** 469–484
8. Whyte, J., Bader, J. R., Tauhata, S. B., Raycroft, M., Hornick, J., Pfister, K. K., Lane, W. S., Chan, G. K., Hinchcliffe, E. H., Vaughan, P. S., and Vaughan, K. T. (2008) *J. Cell Biol.* **183,** 819–834
9. Cheung, P. Y., Zhang, Y., Long, J., Lin, S., Zhang, M., Jiang, Y., and Wu, Z. (2004) *J. Biol. Chem.* **279,** 45308–45311
10. Dixit, R., Levy, J. R., Tokito, M., Ligon, L. A., and Holzbaur, E. L. (2008) *J. Biol. Chem.* **283,** 33611–33619
11. Oshimori, N., Ohsugi, M., and Yamamoto, T. (2006) *Nat. Cell Biol.* **8,** 1095–1101
12. Katsuno, M., Adachi, H., Minamiyama, M., Waza, M., Tokui, K., Banno, H., Suzuki, K., Onoda, Y., Tanaka, F., Doyu, M., and Sobue, G. (2006) *J. Neurosci.* **26,** 12106–12117
13. Soneoka, Y., Cannon, P. M., Ramsdale, E. E., Griffiths, J. C., Romano, G., Kingsman, S. M., and Kingsman, A. J. (1995) *Nucleic Acids Res.* **23,** 628–633
14. Burns, J. C., Friedmann, T., Driever, W., Burrascano, M., and Yee, J. K. (1993) *Proc. Natl. Acad. Sci. U.S.A.* **90,** 8033–8037
15. Kuribara, R., Kinoshita, T., Miyajima, A., Shinjyo, T., Yoshihara, T., Inukai, T., Ozawa, K., Look, A. T., and Inaba, T. (1999) *Mol. Cell. Biol.* **19,** 2754–2762
16. Kuribara, R., Honda, H., Matsui, H., Shinjyo, T., Inukai, T., Sugita, K., Nakazawa, S., Hirai, H., Ozawa, K., and Inaba, T. (2004) *Mol. Cell. Biol.* **24,** 6172–6183
17. Tokai-Nishizumi, N., Ohsugi, M., Suzuki, E., and Yamamoto, T. (2005) *Mol. Biol. Cell* **16,** 5455–5463
18. Shinjyo, T., Kuribara, R., Inukai, T., Hosoi, H., Kinoshita, T., Miyajima, A., Houghton, P. J., Look, A. T., Ozawa, K., and Inaba, T. (2001) *Mol. Cell. Biol.* **21,** 854–864
19. Shi, Q., and King, R. W. (2005) *Nature* **437,** 1038–1042
20. Lu, Y., Wang, Z., Ge, L., Chen, N., and Liu, H. (2009) *Cell Struct. Funct.* **34,** 31–45
21. Echeverri, C. J., Paschal, B. M., Vaughan, K. T., and Vallee, R. B. (1996) *J. Cell Biol.* **132,** 617–633

Leukemia Research 35 (2011) 516–521

Contents lists available at ScienceDirect

Leukemia Research

journal homepage: www.elsevier.com/locate/leukres

Aberrant methylation of the *RIZ1* gene in myelodysplastic syndrome and acute myeloid leukemia

Naoki Mori[a,*], Kentaro Yoshinaga[a], Kaori Tomita[a], Mari Ohwashi[a], Toshiaki Kondoh[a], Hanae Shimura[a], Yan-Hua Wang[a], Masayuki Shiseki[a], Michiko Okada[b], Toshiko Motoji[a]

[a] *Department of Hematology, Tokyo Women's Medical University, 8-1 Kawada-cho, Shinjuku-ku, Tokyo 162-8666, Japan*
[b] *Chromosome Laboratory, Shiseikai Daini Hospital, Tokyo, Japan*

ARTICLE INFO

Article history:
Received 10 June 2010
Received in revised form 25 July 2010
Accepted 3 August 2010
Available online 9 September 2010

Keywords:
Myelodysplastic syndrome
Acute myeloid leukemia
Methylation
RIZ1
Tumor suppressor gene
Epigenetics

ABSTRACT

We performed methylation specific PCR analysis on the *RIZ1* promoter in MDS and AML. Methylation was detected in 17 of 34 MDS (50%) and 22 of 72 AML (31%) ($p = 0.053$). Methylation was detected in eleven of 17 secondary AML from MDS (65%), and eleven of 55 de novo AML (20%) ($p = 0.0005$). Bisulfite sequence revealed methylation at many CpG sites in the promoter. Decreased *RIZ1* expression was accompanied by methylation in six of nine samples examined, while it was also observed in seven of 13 without methylation. Treatment of AML cells, that have *RIZ1* methylation, with 5-Aza-dC, induced growth suppression with *RIZ1* restoration. Our results suggest that the *RIZ1* gene is inactivated in MDS and AML in part by methylation, whereas another mechanism should be involved in others.

1. Introduction

Several lines of evidence have shown that inactivation of tumor suppressor genes is closely associated with tumorigenesis in a wide variety of human tumors [1]. Loss of heterozygosity (LOH) has been reported to occur in various chromosomal regions in diverse tumor types. Moreover, tumor suppressor genes have been identified in some of these regions where frequent LOH has been found in tumors. The two-mutation hypothesis suggests that both alleles of a tumor suppressor gene are inactivated in tumors [2]. Inactivation of a tumor suppressor gene is often caused by a mutation, small deletion of one allele accompanied by loss of the second allele. Furthermore, methylation in a promoter CpG of several tumor suppressor genes has recently been reported and has been associated with loss or decreased expression in many tumors.

Myelodysplastic syndrome (MDS) comprises a heterogeneous group of hematological disorders [3,4]. Patients with MDS often exhibit increased blast counts in the peripheral blood and bone marrow, showing a transition to a more advanced MDS subtype, with eventual development of acute myeloid leukemia (AML). We have previously reported frequent LOH on the short arm of chromosome 1 (1p) in the progression of MDS to AML as well as blast crisis of chronic myelocytic leukemia (CML) [5,6]. Common regions of LOH were subsequently determined in these hematological neoplasms [7,8]. Deletion or LOH on 1p has been one of the most frequent abnormalities observed in a variety of human neoplasms [9,10]. However the target tumor suppressor gene has not been clearly identified for these regions in the neoplasms [11].

The retinoblastoma protein-interacting zinc finger gene *RIZ* was isolated in a functional screening for Rb-binding proteins [12]. The *RIZ* gene maps to 1p36. RIZ contains the canonical Rb-binding motif LXCXE and the nuclear hormone receptor-binding motif LXXLL. RIZ also contains a novel protein methyltransferase domain, called the PR domain or SET domain. The *RIZ* gene encodes two products: RIZ1 contains the PR domain and RIZ2 lacks the domain [13]. RIZ1 but not RIZ2 has tumor-suppressive properties. *RIZ1* expression, but not *RIZ2* expression, is silenced in many types of tumors, including breast cancer, liver cancer, colon cancer, and neuroblastoma [14]. Moreover, inactivation of the *RIZ1* gene by promoter hypermethylation has been reported in breast, liver, and gastric carcinoma [15]. Mouse gene knockout models show that *RIZ1* inactivation can cause tumor susceptibility [16]. Thus, the *RIZ1* gene is one of the candidate tumor suppressor genes on 1p. Previous study showed altered expression of the *RIZ1* gene in human leukemia [17]. However, methylation status of the *RIZ1* gene has not been well studied in hematological neoplasms. To determine the relevance of the *RIZ1* methylation, we performed methylation specific polymerase chain reaction (MS-PCR) analysis on the *RIZ1* gene in 34 patients with

* Corresponding author. Tel.: +81 3 3353 8111x31544; fax: +81 3 5269 7329.
E-mail address: mori@dh.twmu.ac.jp (N. Mori).

0145-2126/$ – see front matter © 2010 Elsevier Ltd. All rights reserved.
doi:10.1016/j.leukres.2010.08.002

Table 1
Clinical characteristics and incidence of *RIZ1* methylation in MDS and AML.

	MDS	Secondary AML	de novo AML
No.	34	17	55
Age, median (range)	66.5 (18–84)	68 (38–85)	50 (21–80)
Sex			
Male	22	11	30
Female	12	6	25
Blast%, median (range)	5.85 (0–29.1)	58.8 (20–95)	77.2 (18–98.4)
	No. of methylation		No. of patient
MDS			
RA	7		13
RARS	0		1
RAEB	4		10
RAEB-t	4		6
CMML	2		4
Total	17		34
AML			
Secondary AML	11		17
De novo AML			
M0	1		1
M1	2		12
M2	1		17
M3	3		7
M4	2		8
M5	1		7
M6	0		1
M7	1		2
Total	11		55
		Frequency of methylation	
MDS			
IPSS score			$p=0.419$
Low		1/4 (25%)	
Intermediate-1		5/10 (50%)	
Intermediate-2		6/11 (55%)	
High		5/9 (56%)	
Karyotype (IPSS)			$p=0.439$
Good		7/12 (58%)	
Intermediate		4/8 (50%)	
Poor		6/14 (43%)	
AML (secondary AML and de novo AML)			
Karyotype (MRC)			$p=0.282$
Favorable		5/16 (31%)	
Intermediate		7/33 (21%)	
Adverse		9/21 (43%)	
Low risk MDS vs. high risk MDS		50% vs. 50%	$p=1$
MDS vs. AML (secondary AML and de novo AML)		50% vs. 31%	$p=0.053$
MDS vs. secondary AML		50% vs. 65%	$p=0.320$
MDS vs. de novo AML		50% vs. 20%	$p=0.003$
Secondary AML vs. de novo AML		65% vs. 20%	$p=0.0005$
	Methylation(+) vs. methylation(−)		
MDS			
Overall survival (3 years)	41% vs. 42%		$p=0.659$
Progression to AML	24% vs. 12%		$p=0.328$
AML			
Overall survival (3 years)	19% vs. 35%		$p=0.192$
Refractoriness to chemotherapy	47% vs. 19%		$p=0.992$

MDS and 17 with AML evolved from MDS (secondary AML) as well as 55 patients with de novo AML.

2. Materials and methods

2.1. Samples

Bone marrow or peripheral blood samples were obtained from 34 patients with MDS, 17 patients with secondary AML from MDS, and 55 patients with de novo AML (Table 1). Mononuclear cells were isolated from bone marrow or peripheral blood by Ficoll–Conray gradient centrifugation. The 34 MDS samples consisted of 13 refractory anemia (RA), 1 RA with ringed sideroblasts (RARS), 10 RA with excess of blasts (RAEB), 6 RAEB in transformation (RAEB-t), 4 chronic myelomonocytic leukemia (CMML). MDS was classified according to the French–American–British (FAB) classification [18]. The 55 AML consisted of 1 M0, 12 M1, 17 M2, 7 M3, 8 M4, 7 M5, 1 M6, and 2 M7 according to the FAB classification. Written informed consent was obtained from the patients. This study was approved by ethics committee of our institute. Clinical information is shown in Table 1. The median percentage of blasts was 5.85% (range, 0–29.1) in MDS. The median percentage of blasts in secondary AML was 58.8% (range, 20–95) and that in de novo AML was 77.2% (range, 18–98.4).

2.2. Cytogenetic analysis

Cytogenetic analysis was performed according to standard methods. Chromosome preparations were Q-banded, and karyotypes were described according to the International System for Human Cytogenetic Nomenclature (ISCN2005). Thirty metaphases were evaluated in most samples. Patients were categorized in risk groups according to the International Prognostic Scoring System (IPSS) for MDS, and the Medical Research Council (MRC) for AML [19,20].

2.3. Cell culture

HL-60 and U-937 myeloid leukemia cells were grown in RPMI 1640 supplemented with 10% fetal calf serum in a 5% CO_2 environment. Leukemia cells (2×10^5/ml) were cultivated for 3 days in the presence of various concentrations of 5-Aza-dC (Wako, Osaka, Japan). Cell culture and 5-Aza-dC treatment were repeated three times.

2.4. Extraction of DNA

Genomic DNA was prepared by proteinase K digestion and phenol/chloroform extraction or using QIAamp DNA Blood Mini Kit (Qiagen, Valencia, CA, USA).

2.5. MS-PCR analysis on the RIZ1 gene

Genomic DNA was treated with bisulfite using CpGenome DNA Modification Kit (Serologicals Corporation, Norcross, GA, USA). Treated DNA was subject to PCR-amplification with HotStarTaq Master Mix Kit (Qiagen). The sequences of the primers for the *RIZ1* gene were previously published [15]. To amplify methylated DNA, we used primer set RP291MF (GTG GTG GTT ATT GGG CGA CGG C) and RP291MR (GCT ATT TCG CCG ACC CCG ACG). To amplify unmethylated DNA, we used RP291UF (TGG TGG TTA TTG GGT GAT GGT) and RP291UR (ACT ATT TCA CCA ACC CCA ACA). After 15 min at 95 °C, 38 cycles of amplification using 30 s at 95 °C, 30 s at 68 °C and 60 s at 72 °C were performed, with a subsequent 10 min extension at 72 °C. For unmethylated DNA, 35 cycles of amplification at annealing temperature 60 °C were performed. PCR products were subject to 2% agarose gel electrophoresis. In each sample electrophoresis was repeated using independent PCR products. CpGenome Universal Methylated DNA (Serologicals Corporation) was used as a positive control. Normal lymphocyte was used as a negative control. Primers RP291MF and RP291MR amplify 176-base pairs (bp) products, while the size of products using the primers RP291UF and RP291UR is 175-bp.

2.6. Sequence analysis within promoter of the RIZ1 gene

Bisulfite sequence was performed in both directions on MegaBase sequence system (Amersham, Buckingham, UK). Bisulfite treated DNA was amplified with primers RP294F (GGT TGG GTG GTG GTT ATT GGG) and RP295R (CAA AAA CCG CCC TGC GCC ACT CCT TAC C) as described above. PCR products of 260-bp were purified using the QIAQuick PCR Purification Kit (Qiagen) and ligated into pGEM-T vector (Promega, Madison, WI, USA). As a template, one of the plasmid clones containing appropriate PCR products was used for the sequencing reaction. In each case, at least three of the plasmid clones were sequenced.

2.7. Quantitative real time reverse transcriptase-PCR (RT-PCR) analysis on the RIZ1 gene

Total RNA was extracted with TRIZOL (Invitrogen, Carlsbad, CA, USA). Measurement of mRNA levels of *RIZ1* mRNA was based on the TaqMan probe method using ABI PRISM 7700 sequence detector system (Applied Biosystems, Foster City, CA, USA). Real time amplification reaction was performed in a total volume of 25 μl with a concentration of 300 nM for primers and 200 nM for probes. After adding 2.5 μl of cDNA and 12.5 μl of TaqMan Universal PCR Master Mix (Applied Biosystems), samples were amplified in duplicates in each experiment. Serially diluted DNA prepared from Raji cell line was used as a standard curve for *RIZ1*, and internal control gene *GAPDH* (TaqMan Endogeneous Control Kit, Applied Biosystems). All final measurements were normalized with *RIZ1*/*GAPDH* average value for each sample. *RIZ1* and *GAPDH* primers and probes were obtained from Applied Biosystems. To amplify *RIZ1* mRNA the following sequences were used for primers PRTF (5′-ATTGATGCCACTGATCCAGAGA-3′) and PRTR (5′-GCTCTGTTGATTTCCAGTGGGA-3′). The following sequences were used for PR probe:

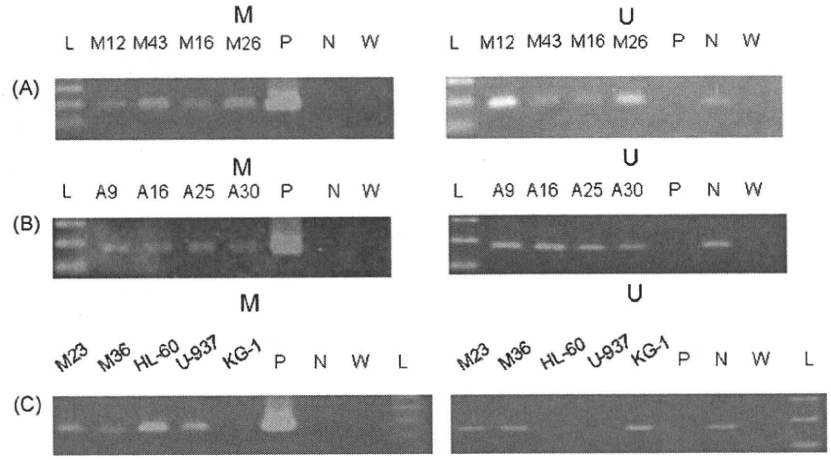

Fig. 1. Methylation of the *RIZ1* gene in MDS and AML. Ten of 25 μl of PCR products were separated by electrophoresis through 2% agarose gel, stained with ethidium bromide and visualized by ultraviolet illumination. M, methylated; U, unmethylated; L, 100-bp ladder; P, positive control; N, negative control; W, water. (A) Methylation was detected in secondary AML (M12, M43, M16), and MDS (M26). Unmethylated band was observed in M12, M43, M16, and M26. (B) Methylation was detected in de novo AML (A9, A16, A25, and A30). Unmethylated band was observed in A9, A16, A25, and A30. (C) Methylation was detected in MDS (M23, M36), HL-60, and U-937. Unmethylated band was observed in M23, M36, and KG-1.

5′-AAACTGGCTGCGATATGTGAATTGGGC-3′ [17]. After 2 min at 50 °C and 10 min at 95 °C, 45 cycles of amplification using 15 s at 95 °C and 60 s at 60 °C were performed.

2.8. Statistical analysis

The correlation between the frequency of *RIZ1* methylation and type of disease or clinical characteristics was analyzed using the chi-square test or Fisher's exact probability test. The correlation between the frequency of *RIZ1* methylation and IPSS or cytogenetic risk groups was analyzed using the Mann–Whitney's *U*-test. Statistical analysis for *RIZ1* expression and methylation was performed with Student's *t*-test or Welch's *t*-test. Analysis was performed using SPSS Software. *p*-Value of less than 0.05 was considered statistically significant.

3. Results

3.1. MS-PCR analysis on the RIZ1 gene in MDS and secondary AML

We first screened 34 samples of MDS and 17 of secondary AML for promoter methylation. Cytogenetic data were available from all the 34 MDS and 15 of the 17 AML patients. Deletions on 1p or monosomy of chromosome 1 was absent in the patients. MS-PCR analysis showed methylation of the *RIZ1* gene in 17 of the 34 samples of MDS (50%) and eleven of 17 secondary AML (65%). Fig. 1A shows examples of methylation. Methylation of the *RIZ1* gene was detected in seven of 14 low risk MDS (50%), 10 of 20 high risk MDS (50%) ($p = 1$, Table 1). Patients with MDS were classified using the IPSS score. Frequency of methylation was not statistically different among IPSS subgroups ($p = 0.419$, Table 1). Frequency of methylation was not statistically different among cytogenetic risk groups ($p = 0.439$, Table 1). No statistical differences were observed between methylation and overall survival (3 years) or progression to AML (Table 1).

3.2. Bisulfite sequence

To define the methylation status of the CpG in the promoter region, we performed bisulfite sequence in several samples with methylation. Bisulfite sequence analysis revealed that methylation was present at many CpG sites in the *RIZ1* promoter region in secondary AML (Fig. 2, M17). Several samples without methylation

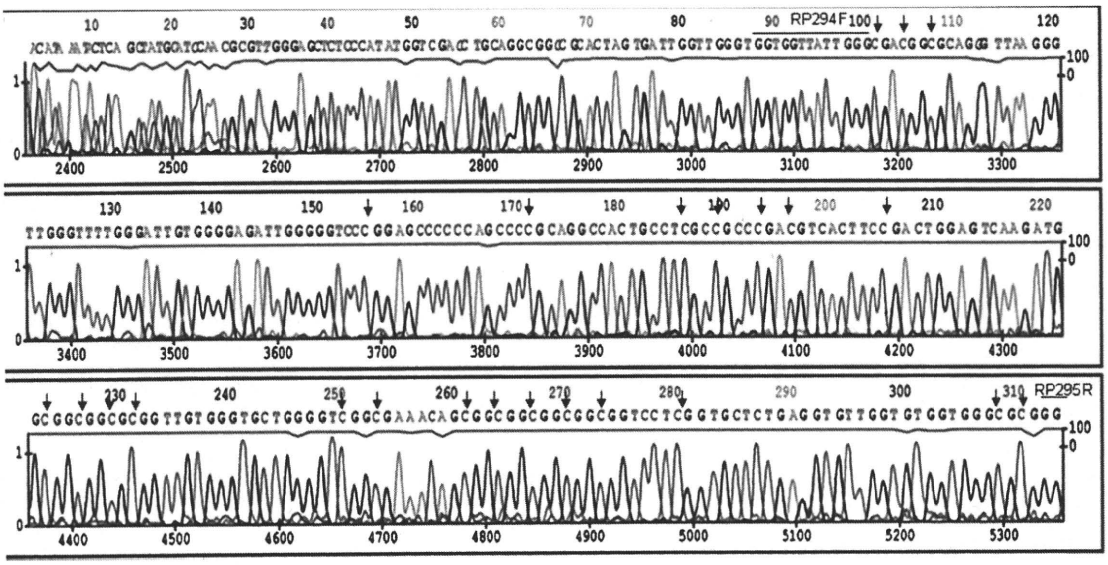

Fig. 2. Methylation was present at many CpG sites in the *RIZ1* gene in secondary AML. Bisulfite sequence analysis was performed at multiple CpG sites in the *RIZ1* promoter region in secondary AML (M17). Arrow indicates methylated cytosine.

by MS-PCR, were also sequenced and no methylated cytosine was observed within the promoter region.

3.3. MS-PCR analysis on the RIZ1 gene in de novo AML

We next analyzed methylation of the *RIZ1* gene in the 55 cases of de novo AML. Cytogenetic data were available from the 55 AML patients. Monosomy 1 accompanied with marker chromosome was observed in one patient without methylation. Methylation was detected in eleven of the 55 de novo AML (20%). Fig. 1B shows examples of methylation in de novo AML. Methylation of the *RIZ1* gene was observed in 1 of the 1 M0, 2 of the 12 M1, 1 of the 17 M2, 3 of the 7 M3, 2 of the 8 M4, 1 of the 7 M5, 0 of the 1 M6, and 1 of the 2 M7 (Table 1). Frequency of methylation was not statistically different among cytogenetic risk groups ($p = 0.282$, Table 1). Methylation was more frequent in MDS than in de novo AML ($p = 0.003$), and in de novo AML and secondary AML ($p = 0.053$), respectively. Methylation was more frequent in secondary AML than in de novo AML ($p = 0.0005$).

3.4. Quantitative real time RT-PCR analysis on the RIZ1 gene in MDS and AML

RNA was available from 27 samples of MDS, secondary AML and de novo AML. Expression of the *RIZ1* gene was examined by quantitative real time RT-PCR analysis in 22 of the 27 samples because of the high quality of RNA. Amplification of the PR region represents expression of the *RIZ1* mRNA.

RIZ1 expression (mean) was not statistically different in secondary AML and de novo AML (2.026 vs. 1.900, $p = 0.815$). *RIZ1* expression (mean) was not statistically different in methylation-positive group and methylation-negative group (1.996 vs. 1.810, $p = 0.728$).

In comparison with expression of normal bone marrow cells, decreased *RIZ1* expression was accompanied by methylation in six of nine samples examined (one of one MDS, three of five secondary AML, and two of three de novo AML) (Fig. 3A and B). Decreased *RIZ1* expression was also observed in seven of 13 without methylation (one of two MDS, one of one secondary AML, and five of 10 de novo AML) (Fig. 3A and B).

3.5. 5-Aza-dC treatment of AML cells

To determine the effect of demethylating agent, HL-60 leukemic cells that have *RIZ1* promoter methylation (Fig. 1C), were cultivated in RPMI. Treatment of HL-60 leukemic cells with 5-Aza-dC resulted in growth suppression and restored *RIZ1* expression (Fig. 4A and B). We also test the effect of 5-Aza-dC with U-937 leukemic cells and similar results were observed.

4. Discussion

Although the molecular genetic changes of MDS have long been studied, the mechanisms responsible for transformation to AML have not been well understood. We have previously reported frequent LOH on 1p in the progression of MDS to AML [5]. Frequent LOH has been reported on 1p in several types of tumors, including neuroblastomas, colorectal, breast and hepatocellular carcinomas, parathyroid adenomas, melanomas, and pheochromocytomas [9,10]. Allelic loss of 1p was associated with unfavorable outcome in neuroblastomas [21]. Our previous study revealed that the consensus regions of allelic loss in MDS resided distal to *D1S253* (1p36), and possibly proximal to *D1S496* (1p32-) [7]. Several candidate genes on 1p have been proposed to be possible targets associated with cancer including *CDC2L1*, *p73*, *TNFR2*, *RIZ1*, *DAN*, *ID3*, *FGR*, and *CHD5* [10–12,22].

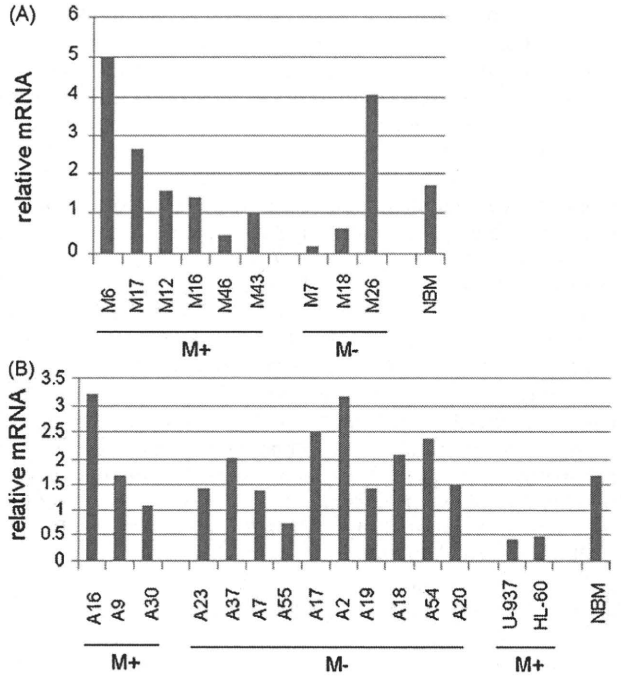

Fig. 3. Quantitative real time RT-PCR analysis of the *RIZ1* gene in MDS and AML. NBM, normal bone marrow. (A) Decreased expression of the *RIZ1* gene was observed in MDS (M46) and secondary AML (M12, M16, and M43) with methylation (M+). Expression of the *RIZ1* gene was also decreased in MDS (M7) and secondary AML (M18), which did not have methylation (M−). (B) Decreased expression of the *RIZ1* gene was observed in de novo AML with methylation (M+) (A9 and A30). Expression of the *RIZ1* gene was also decreased in de novo AML without methylation (M−) (A23, A7, A55, A19, and A20).

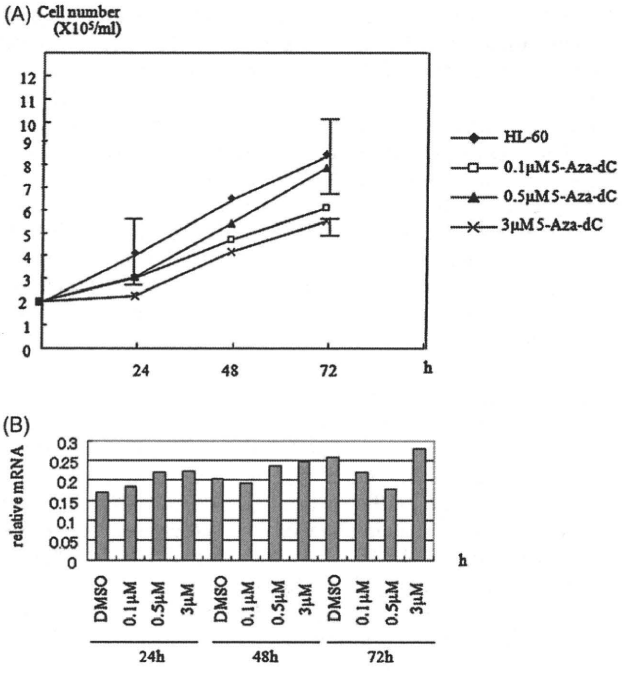

Fig. 4. Treatment of 5-Aza-dC in AML cells. (A) HL-60 cells that have *RIZ1* promoter methylation were treated with 5-Aza-dC. Number of cells (mean) is indicated according to treatment; Bar, SD. (B) Quantitative real time RT-PCR analysis of the *RIZ1* gene. Expression of PR was restored by 5-Aza-dC treatment in HL-60.

DNA methylation in CpG islands represents an important epigenetic modification in neoplasms. Methylation is associated with transcription silencing of genes that function in cell differentiation, apoptosis, growth regulation, cell signaling, conferring selective advantage to the malignant cells. Tumor suppressor genes reported to be methylated in MDS, include the *P15*, *P16*, *E-cadherin*, and *SOCS-1* genes [4]. Although clinical efficacies of hypomethylating agents have been reported in MDS, the basis for the effectiveness has not been well known [4]. Recent study showed methylation in several other genes in MDS [23]. The *FZD9* gene was found to be a frequent target of methylation on chromosome 7 [23]. To elucidate the epigenetic alterations that may inactivate the possible target gene on 1p, we performed MS-PCR of the promoter region of the *RIZ1* gene. The present study revealed frequent methylation of the *RIZ1* promoter region in MDS and secondary AML. Since the incidence of methylation was not statistically different in low risk MDS and high risk MDS, and also in secondary AML, it is suggested that *RIZ1* methylation is a relatively early event. *RIZ1* methylation was found in 62% of liver cancer and 44% of breast cancer cases [15]. Our study demonstrated that *RIZ1* methylation was also frequent in MDS and secondary AML.

The genetic alterations involved in de novo AML have been largely different from those of MDS. Although methylation of the *P15*, *P16*, *E-cadherin*, and *SOCS-1* genes was also reported in de novo AML, recent study revealed methylation in other genes in AML [24]. Thus, we next analyzed methylation of the *RIZ1* gene in de novo AML. In comparison with MDS and secondary AML, relatively lower incidence of the *RIZ1* methylation was found in de novo AML (20%). Frequency of methylation was not statistically different among IPSS subgroups or cytogenetic risk groups in MDS, and it was not significant among cytogenetic risk groups in AML.

Irrespective of frequent methylation in MDS and secondary AML, *RIZ1* expression (mean) was not statistically different in secondary AML and de novo AML. In addition, *RIZ1* expression (mean) was not statistically different in methylation-positive and methylation-negative MDS and AML. Previous study reported that the *RIZ1* expression was decreased or absent in AML [17]. In the current study, quantitative real time RT-PCR analysis revealed decreased expression of the *RIZ1* in many of MDS and AML with methylation. In contrast, several samples with methylation did not show the decreased *RIZ1* expression. A similar observation was found in gastric carcinoma [25]. These differences may be related to the high sensitivity of MS-PCR. Alternatively, possible contamination of normal cells in the samples may account for the expression. Another explanation is that methylation may be partially involved in malignant cells, since some of these samples were supposed to contain more than 90% blast cells after mononuclear cell isolation. On the other hand, some other samples without methylation showed decreased *RIZ1* expression. Another mechanism inactivating RIZ1, such as deletions, defect in certain transcription factor, histone methylation or miRNA may be involved in MDS and AML without promoter methylation.

5-Aza-dC treatment of HL-60 and U-937 cells showed suppression of cell proliferation together with restoration of the *RIZ1* expression. Since the restoration was not prominent, promoter methylation may not be well correlated with the decreased expression in these cells. However, as mentioned earlier, *RIZ1* inactivation can cause tumor susceptibility [16]. Moreover, recent study revealed that forced expression of *RIZ1* in CML blast crisis cell line decreased proliferation, increased apoptosis and enhanced differentiation [26]. Therefore, although another gene(s) restored by 5-Aza-dC may also play a role in the suppressive effect, our results suggest that the *RIZ1* gene is one of the target tumor suppressor genes on 1p inactivated in MDS and AML. Further study revealing the mechanism of RIZ1 inactivation without promoter methylation will help understand the genesis of disease progression and develop a new therapeutic strategy in MDS and AML.

Acknowledgements

This work was supported in part by a grant-in-aid from the Ministry of Health, Labour, and Welfare of Japan. This work was supported in part by a grant-in-aid from the International Research and Educational Institute for Integrated Medical Sciences (IREIIMS) of Tokyo Women's Medical University.

Contributions. NM designed the study, performed the experimental research, and wrote the paper. KY helped with the design of the study and collecting samples. KT and MO helped with collecting samples, the MS-PCR, the quantitative real time RT-PCR, and cell culture. TK helped with collecting samples and the MS-PCR. HS helped with collecting samples and the quantitative real time RT-PCR. Y-HW helped with the sequencing. MO performed the cytogenetic analysis. MS and TM helped with the design of the study.

Conflict of interest statement

The authors declare no conflict of interest regarding this article.

References

[1] Weinberg RA. Tumor suppressor genes. Science 1991;254:1138–46.
[2] Knudson AG. Mutation and cancer: statistical study of retinoblastoma. Proc Natl Acad Sci USA 1971;68:820–3.
[3] Koeffler HP. Myelodysplastic syndromes (preleukemia). Semin Hematol 1986;23:284–99.
[4] Nimer SD. Myelodysplastic syndromes. Blood 2008;111:4841–51.
[5] Mori N, Morosetti R, Hoflehner E, Lubbert M, Mizoguchi H, Koeffler HP. Allelicloss in the progression of myelodysplastic syndrome. Cancer Res 2000;60:3039–42.
[6] Mori N, Morosetti R, Lee S, Spira S, Ben-Yehuda D, Schiller G, et al. Allelotype analysis in the evolution of chronic myelocytic leukemia. Blood 1997;90:2010–4.
[7] Mori N, Morosetti R, Mizoguchi H, Koeffler HP. Progression of myelodysplastic syndrome: allelic loss on chromosomal arm 1p. Br J Haematol 2003;122:226–30.
[8] Mori N, Morosetti R, Spira S, Lee S, Ben-Yehuda D, Schiller G, et al. Chromosome band 1p36 contains a putative tumor suppressor gene important in the evolution of chronic myelocytic leukemia. Blood 1998;92:3405–9.
[9] Dracopoli NC, Harnett P, Bale SJ, Stanger BZ, Tucker MA, Housman DE, et al. Loss of alleles from the distal short arm of chromosome 1 occurs late in melanoma tumor progression. Proc Natl Acad Sci USA 1989;86:4614–8.
[10] Schwab M, Praml C, Amler LC. Genomic instability in 1p and human malignancies. Genes Chromosom Cancer 1996;16:211–29.
[11] Bagchi A, Mills AA. The quest for the 1p36 tumor suppressor. Cancer Res 2008;68:2551–6.
[12] Buyse IM, Shao G, Huang S. The retinoblastoma protein binds to RIZ, a zinc-finger protein that shares an epitope with the adenovirus E1A protein. Proc Natl Acad Sci USA 1995;92:4467–71.
[13] He L, Yu JX, Liu L, Buyse IM, Wang MS, Yang QC, et al. RIZ1, but not the alternative RIZ2 product of the same gene, is underexpressed in breast cancer, and forced RIZ1 expression causes G2-M cell cycle arrest and/or apoptosis. Cancer Res 1998;58:4238–44.
[14] Chadwick RB, Jiang G-L, Bennington GA, Yuan B, Johnson CK, Stevens MW, et al. Candidate tumor suppressor RIZ is frequently involved in colorectal carcinogenesis. Proc Natl Acad Sci USA 2000;97:2662–7.
[15] Du Y, Carling T, Fang W, Piao Z, Sheu J-C, Huang S. Hypermethylation in human cancers of the RIZ1 tumor suppressor gene, a member of a histone/protein methyltransferase superfamily. Cancer Res 2001;61:8094–9.
[16] Steele-Perkins G, Fang W, Yang X-H, Van Gele M, Carling T, Gu J, et al. Tumor formation and inactivation RIZ1, an Rb-binding member of a nuclear protein-methyltransferase superfamily. Genes Dev 2001;15:2250–62.
[17] Sasaki O, Meguro K, Tohmiya Y, Funato T, Shibahara S, Sasaki T. Altered expression of retinoblastoma protein-interacting zinc finger gene RIZ, in human leukaemia. Br J Haematol 2002;119:940–8.
[18] Bennet JM, Catovsky D, Daniel MT, et al. Proposals for the classification of the myelodysplastic syndromes. Br J Haematol 1982;51:189–99.
[19] Greenberg P, Cox C, Le Beau MM, Fenaux P, Morel P, Sanz G, et al. International scoring system for evaluating prognosis in myelodysplastic syndromes. Blood 1997;89:2079–88.

[20] Grimwade D, Walker H, Oliver F, Wheatley K, Harrison C, Harrison G, et al. The importance of diagnostic cytogenetics on outcome in AML: analysis of 1612 patients entered into the MRC AML 10 trial. The Medical Research Council Adult and Children's Leukemia Working Parties. Blood 1998;92:2322–33.
[21] Caron H, van Sluis P, de Kraker J, Bokkerink J, Egeler M, Laureys G, et al. Allelic loss of chromosome 1p as a predictor of unfavorable outcome in patients with neuroblastoma. N Engl J Med 1996;334:225–30.
[22] Kaghad M, Bonnet H, Yang A, Creancier L, Biscan J-C, Valent A, et al. Monoallelically expressed gene related to p53 at 1p36, a region frequently deleted in neuroblastoma and other human cancers. Cell 1997;90:809–19.
[23] Jiang Y, Dunbar A, Gondek LP, Mohan S, Rataul M, O'Kneefe C, et al. Aberrant DNA methylation is a dominant mechanism in MDS progression to AML. Blood 2009;113:1315–25.
[24] Kroeger H, Jelinek J, Estecio MRH, He R, Kondo K, Chung W, et al. Aberrant CpG island methylation in acute myeloid leukemia is accentuated at relapse. Blood 2008;112:1366–73.
[25] Oshimo Y, Oue N, Mitani Y, Nakayama H, Kitadai Y, Yoshida K, et al. Frequent epigenetic inactivation of RIZ1 by promoter hypermethylation in human gastric carcinoma. Int J Cancer 2004;110:212–8.
[26] Pastural E, Takahashi N, Dong W-F, Bainbridge M, Hull A, Pearson D, et al. RIZ1 repression is associated with insulin-like growth factor-1 signaling activation in chronic myeloid leukemia cell lines. Oncogene 2007;26:1586–94.

Int J Hematol (2010) 92:111–117
DOI 10.1007/s12185-010-0621-x

ORIGINAL ARTICLE

Imatinib for newly diagnosed chronic-phase chronic myeloid leukemia: results of a prospective study in Japan

Tadashi Nagai · Jin Takeuchi · Nobuaki Dobashi · Yuzuru Kanakura · Shuichi Taniguchi · Koji Ezaki · Chiaki Nakaseko · Akira Hiraoka · Masaya Okada · Yasushi Miyazaki · Toshiko Motoji · Masaaki Higashihara · Norifumi Tsukamoto · Hitoshi Kiyoi · Shinji Nakao · Katsuji Shinagawa · Ryuzo Ohno · Tomoki Naoe · Kazunori Ohnishi · Noriko Usui

Received: 22 December 2009 / Revised: 7 May 2010 / Accepted: 31 May 2010 / Published online: 25 June 2010

Abstract Although imatinib has become the current standard treatment for chronic myeloid leukemia (CML), there is limited information regarding its efficacy and safety among Japanese patients. We therefore conducted a prospective multi-center open-label study of imatinib for Japanese patients with newly diagnosed chronic-phase CML (CP-CML). A total of 107 patients were enrolled and treated with imatinib at an initial daily dose of 400 mg. Eighty-three patients completed 3 years of study treatment. The cumulative rates of major cytogenetic response and complete cytogenetic response (CCyR) were 90.9 and 90.2% at 3 years, respectively. The safety profile was not very different from that reported in the IRIS study, although grade ≥3 neutropenia occurred relatively frequently (31.8 vs. 14.3%). Only seven patients discontinued the study due to adverse events, as did four patients due to

T. Nagai and J. Takeuchi contributed equally to this study, and the order in which they are listed should be considered arbitrary.

T. Nagai (✉)
Division of Hematology, Jichi Medical University Hospital, Shimotsuke 329-0498, Japan
e-mail: t-nagai@jichi.ac.jp

J. Takeuchi
Nihon University Itabashi Hospital, Tokyo, Japan

N. Dobashi · N. Usui
Jikei University Hospital, Tokyo, Japan

Y. Kanakura
Osaka University Hospital, Osaka, Japan

S. Taniguchi
Toranomon Hospital, Tokyo, Japan

K. Ezaki
Fujita Health University Hospital, Toyoake, Japan

C. Nakaseko
Chiba University Hospital, Chiba, Japan

A. Hiraoka
Osaka Medical Center for Cancer and Cardiovascular Diseases, Osaka, Japan

M. Okada
The Hospital of Hyogo College of Medicine, Hyogo, Japan

Y. Miyazaki
Nagasaki University Hospital, Nagasaki, Japan

T. Motoji
Tokyo Women's Medical University, Tokyo, Japan

M. Higashihara
Kitasato University Hospital, Sagamihara, Japan

N. Tsukamoto
Gunma University Hospital, Maebashi, Japan

H. Kiyoi · T. Naoe
Nagoya University Hospital, Nagoya, Japan

S. Nakao
Kanazawa University Hospital, Kanazawa, Japan

K. Shinagawa
Okayama University Hospital, Okayama, Japan

R. Ohno
Aichi Cancer Center, Nagoya, Japan

K. Ohnishi
Hamamatsu University School of Medicine, Hamamatsu, Japan

insufficient efficacy. The 3-year probabilities of overall survival and progression-free survival were 93.2 and 91.4%, respectively. Higher average daily doses (i.e., ≥350 mg) were significantly associated not only with higher rates of achieving CCyR, but also with longer duration of CCyR. These findings confirm the clinical utility of imatinib in Japanese patients with newly diagnosed CP-CML, and suggest detrimental effect of low average daily dose on treatment results.

Keywords Chronic myeloid leukemia · Chronic phase · Newly diagnosed · Imatinib

1 Introduction

Imatinib is a molecule-targeting drug that inhibits BCR-ABL tyrosine kinase and exerts a selective proliferation-inhibitory effect in chronic myeloid leukemia (CML) [1, 2]. Several international trials have documented excellent clinical efficacy of imatinib in patients with chronic-phase CML (CP-CML) [3–5], as well as in patients in accelerated phase (AP) [6] and blast crisis (BC) [7]. Based on those studies along with Japanese phase I and phase II studies [8], imatinib was approved in Japan in November 2001, and has been available in clinical practice since December 2001. However, there is very limited information regarding efficacy and safety of imatinib among Japanese patients. We therefore conducted a post-marketing study to confirm clinical utility of imatinib in Japanese patients with newly diagnosed CP-CML.

2 Patients and methods

2.1 Study design

This was a prospective, multi-center, non-controlled study to evaluate efficacy and safety of imatinib in Japanese patients 15–74 years of age with Philadelphia chromosome positive (Ph+) CP-CML. Eligible patients were those with Eastern Cooperative Oncology Group performance status 0–3 who had been previously untreated with interferon (IFN) or imatinib. Patients were excluded if serum bilirubin or serum creatinine levels were ≥3 times the upper limit of the normal range, if serum aspartate aminotransferase (AST) or alanine aminotransferase (ALT) levels were ≥5 times the upper limit of the normal range, if they received hydroxycarbamide within a week prior to enrollment or any other antileukemic drug within 2 weeks, or if there was any evidence of AP or BC in association with any of the following conditions: ≥15% blasts in the peripheral blood or bone marrow; ≥30% blasts plus promyelocytes in the peripheral blood or bone marrow; ≥20% basophils in the peripheral blood; or extramedullary leukemic infiltrates with the exception of spleen or liver. Women who were pregnant or possibly pregnant were also excluded.

Patients were treated with imatinib at a daily dose of 400 mg. Dose escalation to 600 mg was implemented if they had failed to achieve complete hematologic response (CHR) at 3 months or major cytogenetic response (MCyR) at 6 months. If the patient had failed to achieve MCyR at 9 months, IFN was started at a daily dose of 300 million unit per body two or three times a week while on imatinib. Dose modification of imatinib was generally based on the following guidelines. For grade ≥3 liver dysfunction (elevated bilirubin, AST, or ALT), administration was interrupted until recovery to grade <2, and then resumed at 300 mg/day. For grade ≥3 neutropenia or thrombocytopenia, administration was interrupted until recovery to grade <2, and then resumed at 400 mg/day. If grade ≥3 toxicity recurred after resuming, dose reduction to 300 mg/day was implemented. The study was discontinued in the event of failure to achieve CHR at 6 months, intolerance to imatinib, disease progression to AP or BC, death, patient request, and lost to follow-up, or at the discretion of the investigator. Patients were followed up to 3 years from the day of starting imatinib.

2.2 Endpoints

The primary endpoints were overall survival (OS) and progression-free survival (PFS). OS was defined as the time from the day of first dose of imatinib to death or last follow-up, and PFS was defined as the time from the day of first dose of imatinib to progression to AP or BC, death or last follow-up. Secondary endpoints were hematologic, cytogenetic and molecular response, and adverse events. Cytogenetic response was assessed by using bone marrow cells every 3 months until 12 months and every 6 months thereafter until 36 months. Complete cytogenetic response (CCyR) was defined as complete disappearance of the Philadelphia chromosome. MCyR was defined as decrease in Philadelphia chromosome to 35% or lower. Adverse events were assessed according to the National Cancer Institute Common Toxicity Criteria version 2.0.

Cumulative rates of hematologic and cytogenetic response, PFS, event-free survival (EFS), and OS were evaluated in accordance with the IRIS study reports [3, 9]. EFS was defined as the time from the day of first dose of imatinib to death, progression to AP or BC, loss of CHR, loss of MCyR, increase in white blood cell count to 20000/μL, or last follow-up.

This study was conducted in compliance with the Declaration of Helsinki and was approved by local Institutional Review Boards. All patients provided written informed consent prior to initiation of study medication.